

# We are IntechOpen, the world's leading publisher of Open Access books Built by scientists, for scientists

4,800

Open access books available

122,000

International authors and editors

135M

Downloads

Our authors are among the

154

Countries delivered to

TOP 1%

most cited scientists

12.2%

Contributors from top 500 universities



WEB OF SCIENCE™

Selection of our books indexed in the Book Citation Index  
in Web of Science™ Core Collection (BKCI)

Interested in publishing with us?  
Contact [book.department@intechopen.com](mailto:book.department@intechopen.com)

Numbers displayed above are based on latest data collected.  
For more information visit [www.intechopen.com](http://www.intechopen.com)



# Theory of Fuel Life Control Methods at Nuclear Power Plants (NPP) with Water-Water Energetic Reactor (WWER)

Sergey Pelykh and Maksim Maksimov  
*Odessa National Polytechnic University, Odessa  
Ukraine*

## 1. Introduction

The problem of fuel life control at nuclear power plants (NPP) with WWER-type light-water reactors (PWR) will be discussed for design (normal) loading conditions only. That is, emergency nuclear reactor (NR) operation leading to cladding material plastic deformation is not studied here, therefore the hot plasticity (stress softening) arising at the expense of yield stress decrease under emergency cladding temperature rise, will not be considered here.

Analysing the current Ukrainian energetics status it is necessary to state that on-peak regulating powers constitute 8 % of the total consolidated power system (CPS), while a stable CPS must have 15 % of on-peak regulating powers at least. More than 95 % of all thermal plants have passed their design life and the Ukrainian thermal power engineering averaged remaining life equals to about 5 years. As known, the nuclear energetics part in Ukraine is near 50 %. Hence, operation of nuclear power units of Ukraine in the variable part of electric loading schedule (variable loading mode) has become actual recently, that means there are repeated cyclic NR capacity changes during NR normal operation.

Control of fuel resource at WWER nuclear units is a complex problem consisting of a few subproblems. First of all, a physically based fuel cladding failure model, fit for all possible regimes of normal NR operation including variable loading and burnups above 50 MW·d/kg, must be worked out. This model must use a certified code developed for fuel element (FE) behaviour analysis, which was verified on available experimental data on cladding destruction.

The next condition for implementation of nuclear fuel resource control is availability of a verified code estimating distribution of power flux in the active core for any reactor normal operation mode including variable loading.

It should be noticed that calculation of nuclear fuel remaining life requires estimating change of the state of a fuel assembly (FA) rack. For instance, the state of a rack can change considerably at core disassembling (after a design accident) or at spent fuel handling. Generally speaking, the total fuel handling time period must be considered including the duration of dry/wet storage. Before designing a nuclear fuel resource control system, using

probability theory and physically based FA failure criteria, the failure probability for all FA must be estimated. Having satisfied the listed conditions, a computer-based system for control of nuclear fuel remaining life can be worked out.

The FEMAXI code has been used to calculate the cladding stress/strain development for such its quality as simultaneous solution of the FE heat conduction and mechanical deformation equations using the finite element method (FEM) allowing consideration of variable loading (Suzuki, 2000). Sintered uranium dioxide was assumed to be the material of pellets while stress relieved Zircaloy-4 was assumed to be the material of cladding (Suzuki, 2010). Cladding material properties in the FEMAXI code are designated in compliance with (MATPRO-09, 1976). But the manufacturing process and the zircaloy alloy used are not specified here.

FE behaviour for UTVS (the serial FA of WWER-1000, V-320 project), TVS-A (the serial FA of WWER-1000 produced by OKBM named after I.I. Aphrikantov) and TVS-W (the serial FA produced by WESTINGHOUSE) has been analysed.

The full list of input parameters used when analyzing the PWR fuel cladding durability can be seen in (Suzuki, 2000). The NR regime and FA constructional parameters were set in compliance with Shmelev’s method (Shmelev et al., 2004). The main input parameters of FE and FA used when analyzing the WWER-1000 fuel cladding durability are listed in Table 1.

Parameter	TVS		
	UTVS	TVS-A	TVS-W
Cladding outer diameter, cm	0.910	0.910	0.914
Cladding inner diameter, cm	0.773	0.773	0.800
Cladding thickness, cm	0.069	0.069	0.057
Pellet diameter, cm	0.757	0.757	0.784
Pellet centre hole diameter, cm	0.24	0.14	—
Pellet dish	—	—	each side
Equivalent coolant hydraulic diameter, cm	1.06	1.06	1.05
Total fuel weight for a FE, kg	1.385	1.487	1.554

Table 1. Different parameters of UTVS, TVS-A and TVS-W.

FE cladding rupture life control for a power-cycling nuclear unit having the WWER-1000 NR is a key task in terms of rod design and reliability. Operation of a FE is characterized by

long influence of high-level temperature-power stressing leading to uncontrollable cladding material creep processes causing, after a while, its destruction, and fission products enter the circuit in the quantities exceeding both operational limits and limits of safe operation. In this connection, estimation of cladding integrity time for a NR variable loading mode, taking into account some appointed criteria, becomes one of key problems of FE designing and active core operational reliability analysis.

In accordance with the experience, there are following main characteristic cladding destruction mechanisms for the WWER-1000 varying loading mode (Suzuki, 2010): pellet-cladding mechanical interaction (PCMI), especially at low burnups and stress corrosion cracking (SCC); corrosion at high burnups (>50 MWd/kg-U); cladding failure caused by multiple cyclic and long-term static loads.

It is supposed that influence of low-burnup PCMI is eliminated by implementation of the WWER-1000 maximum linear heat rate (LHR) regulation conditions. Non-admission of cladding mechanical damage caused by SCC is ensured by control of linear heat power permissible values and jumps also. The high-burnup corrosion influence is eliminated by optimization of the alloy fabrication technique.

As all power history affects fuel cladding, it is incorrect to transfer experimental stationary and emergency operation cladding material creep data onto the FE cladding working at variable loading. Emergency NR operation leading to cladding material plastic deformation is not studied here, therefore hot plasticity (stress softening) arising at the expense of yield stress decrease under emergency cladding temperature rise, is not considered.

To solve this problem, we are to define main operating conditions affecting FE cladding durability and to study this influence mechanism. The normative safety factor  $K_{\text{norm}}$  for cladding strength criteria is defined as

$$K_{\text{norm}} = R^{\text{max}} / R, \quad (1)$$

where  $R^{\text{max}}$  is the limit value of a parameter;  $R$  is the estimated value of a parameter.

The group of WWER-1000 cladding strength criteria includes the criteria SC1...SC5 – see Table 2 (Novikov et al., 2005). According to SC4, the WWER-1000 FE cladding total damage parameter is usually estimated by the relative service life of cladding, when steady-state operation and varying duty are considered separately:

$$\omega(\tau) = \sum_i \frac{NC_i}{NC_i^{\text{max}}} + \int_0^\tau \frac{dt}{t^{\text{max}}} < 1, \quad (2)$$

where  $\omega(\tau)$  is the cladding material damage parameter;  $NC_i$  and  $NC_i^{\text{max}}$  are the number of  $i$ -type power-cycles and the allowable number of  $i$ -type power-cycles, respectively;  $t$  is time;  $t^{\text{max}}$  is the creep-rupture life under steady-state operation conditions.

The cladding material damage parameter can be considered as a structure parameter describing the material state ( $\omega = 0$ , for the intact material and  $\omega = 1$ , for the damaged

material). The second possible approach is considering  $\omega(\tau)$  as a characteristic of discontinuity flaw. That is when  $\omega = 0$ , there are no submicrocracks in the cladding material. But if  $\omega = 1$ , it is supposed that the submicrocracks have integrated into a macrocrack situated in some cross-section of the cladding

Criterion	Definition	$K_{\text{norm}}$
SC1	$\sigma_{\theta}^{\text{max}} \leq 250 \text{ MPa}$ , where $\sigma_{\theta}^{\text{max}}$ is maximum circumferential stress.	1.2
SC2	$\sigma_e^{\text{max}} < \sigma_0(T, \phi)$ , where $\sigma_e^{\text{max}}$ is maximum equivalent stress, Pa; $\sigma_0$ is yield stress, Pa; $T$ is temperature, K; $\phi$ is neutron fluence, $\text{cm}^{-2} \cdot \text{s}^{-1}$ .	-
SC3	$P_c \leq P_c^{\text{max}}$ , where $P_c$ is coolant pressure, Pa.	1.5
SC4	$\omega(\tau) = \sum_i \frac{NC_i}{NC_i^{\text{max}}} + \int_0^{\tau} \frac{dt}{t^{\text{max}}} < 1.$	10
SC5	$\varepsilon_{\theta, pl}^{\text{max}} \leq 0.5 \%$ , where $\varepsilon_{\theta, pl}^{\text{max}}$ is cladding limit circumferential plastic strain	-

Table 2. Cladding strength criteria.

An experimental study of Zircaloy-4 cladding deformation behavior under cyclic pressurization (at 350 °C) was carried out in (Kim et al., 2007). The investigated cladding had an outer diameter and thickness of 9.5 mm and 0.57 mm, respectively. The microstructure of Zircaloy-4 was a stress-relieved state. A sawtooth pressure waveform was applied at different rates of pressurization and depressurization, where the maximum hoop stress was varied from 310 MPa to 470 MPa, while the minimum hoop stress was held constant at 78 MPa. Using the cladding stress-life diagram and analyzing the metal structure and fatigue striation appearance, it was found that when loading frequency  $\nu < 1 \text{ Hz}$ , creep was the main mechanism of thin cladding deformation, while the fatigue component of strain was negligibly small.

Taking into account the experimental results (Kim et al., 2007), it can be concluded that estimation of  $\omega(\tau)$  by separate consideration of NR steady-state operation and varying duty (2) has the following disadvantages: the physical mechanism (creep) of cladding damage accumulation and real stress history are not taken into account; uncertainty of the cladding durability estimate forces us into unreasonably assumption  $K_{\text{norm}} = 10$ ; there is no public data on  $N_i^{\text{max}}$  and  $t^{\text{max}}$  for all possible loading conditions.

Now the WWER-1000 fuel cladding safety and durability requirements have not been clearly defined (Semishkin et al., 2009). As strength of fuel elements under multiple cyclic power changes is of great importance when performing validation of a NR project, a tendency to in-depth studies of this problem is observed. The well-known cladding fatigue failure criterion based on the relationship between the maximum circumferential stress amplitude  $\sigma_{\theta}^{\text{max}}$  and the allowable number of power-cycles  $NC^{\text{max}}$  is most popular at present (Kim et al., 2007). Nevertheless, in case of satisfactory fit between the experimental and calculated data

describing the maximum number of cycles prior to the cladding failure, still there stays the problem of disagreement between experimental conditions and real operating environment (e.g. fluence; neutron spectrum; rod internal pressure; coolant temperature conditions; cladding water-side corrosion rate; radiation growth; cladding defect distribution; algorithm of fuel pick-and-place operations; reactor control system regulating unit movement amplitude and end effects; loading cycle parameters, etc.). In connection with this problem, to ensure a satisfactory accuracy of the cladding state estimation at variable loading conditions, it is necessary to develop physically based FE cladding durability analysis methods, on the basis of verified codes available through an international data bank.

As is known, when repair time is not considered, reactor capacity factor CF is obtained as

$$CF = \frac{\sum_{i=1}^n (\Delta \tau_i \cdot P_i)}{T \cdot P}, \quad (3)$$

where  $\Delta \tau_i$  – NR operating time at the capacity of  $P_i$ ;  $T$  – total NR operating time;  $P$  – maximum NR capacity (100 %).

Using (3), the number of daily cycles  $N_{e,0}$  that the cladding can withstand prior to the beginning of the rapid creep stage, expressed in effective days, is defined from the following equation:

$$N_{e,0} = N_0 \cdot CF,$$

where  $N_0$  – the number of calendar daily cycles prior to the beginning of the rapid creep stage.

It should be stressed that CF is a summary number taking into account only the real NR loading history. For instance, the following NR loading modes can be considered:

1. Stationary operation at 100 % NR capacity level,  $CF = 1$ .
2. The NR works at 100 % capacity level within 5 days, then the reactor is transferred to 50 % capacity level within 1 hour. Further the NR works at the capacity level of 50 % within 46 hours, then comes back to 100 % capacity level within 1 hour. Such NR operating mode will be designated as the (5 d – 100 %, 46 h – 50 %) weekly load cycle,  $CF = 0.860$ .
3. The NR works at 100 % capacity level within 16 hours, then the reactor is transferred to 75 % capacity level within 1 hour. Further the NR works at 75 % capacity level within 6 hours, then comes back to 100 % capacity level within 1 hour. Such NR operating mode will be designated as the (16 h – 100 %, 6 h – 75 %) daily load cycle,  $CF = 0.927$ .
4. The NR works at 100 % capacity level within 16 hours, then the reactor is transferred to 75 % capacity level within 1 hour. Further the NR works at 75 % capacity level within 6 hours, then comes back to 100 % capacity level within 1 hour. But the NR capacity decreases to 50 % level within last hour of every fifth day of a week. Further the reactor works during 47 hours at 50 % capacity level and, at last, within last hour of every seventh day the NR capacity rises to the level of 100 %. Such NR operating mode will be designated as the (5 d – 100 % + 75 %, 2 d – 50 %) combined load cycle,  $CF = 0.805$ .



## 2. The CET-method of fuel cladding durability estimation at variable loading

The new cladding durability analysis method, which is based on the creep energy theory (CET) and permits us to integrate all known cladding strength criteria within a single calculation model, is fit for any normal WWER/PWR operating conditions (Pelykh et al., 2008). The CET-model of cladding behaviour makes it possible to work out cladding rupture life control methods for a power-cycling WWER-1000 nuclear unit. As the WWER-1000 Khmelnitskiy nuclear power plant (KhNPP) is a base station for study of varying duty cycles in the National Nuclear Energy Generating Company ENERGOATOM (Ukraine), the second power unit of KhNPP will be considered.

According to CET, to estimate FE cladding running time under multiple cyclic NR power changes, it is enough to calculate the energy  $A_0$  accumulated during the creep process, by the moment of cladding failure and spent for cladding material destruction (Sosnin and Gorev, 1986). The energy spent for FE cladding material destruction is called as specific dispersion energy (SDE)  $A(\tau)$ . The proposed method of FE cladding running time analysis is based on the following assumptions of CET: creep and destruction processes proceed in common and influence against each other; at any moment  $\tau$  creep process intensity is estimated by specific dispersion power (SDP)  $W(\tau)$ , while intensity of failure is estimated by  $A(\tau)$  accumulated during the creep process by the moment  $\tau$

$$A(\tau) = \int_0^{\tau} W(\tau) \cdot d\tau, \quad (4)$$

where SDP standing in (4) is defined by the following equation (Nemirovsky, 2001):

$$W(\tau) = \sigma_e \cdot \dot{p}_e, \quad (5)$$

where  $\sigma_e$  is equivalent stress, Pa;  $\dot{p}_e$  is rate of equivalent creep strain, s<sup>-1</sup>.

Equivalent stress  $\sigma_e$  is expressed as

$$\sigma_e = \sqrt{\frac{1}{2}[(\sigma_{\theta} - \sigma_z)^2 + \sigma_{\theta}^2 + \sigma_z^2]}, \quad (6)$$

where  $\sigma_{\theta}$  and  $\sigma_z$  are circumferential stress and axial stress, respectively.

The cladding material failure parameter  $\omega(\tau)$  is entered into the analysis:

$$\omega(\tau) = A(\tau) / A_0, \quad (7)$$

where  $A_0$  is SDE at the moment of cladding material failure beginning, known for the given material either from experiment, or from calculation, J/m<sup>3</sup> (Sosnin and Gorev, 1986);  $\omega = 0$  – for intact material,  $\omega = 1$  – for damaged material.

The proposed method enables us to carry out quantitative assessment of accumulated  $\omega(\tau)$  for different NR loading modes, taking into account a real NR load history (Pelykh et al., 2008). The condition of cladding material failure is derived from (4), (5) and (7):

$$\omega(\tau) = \int_0^{\tau} \frac{\sigma_e \cdot \dot{p}_e}{A_0} \cdot d\tau = 1 \quad (8)$$

The CET-method of light-water reactor (LWR) FE cladding operation life estimation can be considered as advancement of the method developed for FE cladding failure moment estimation at loss-of-coolant severe accidents (LOCA) (Semishkin, 2007). The equations of creep and cladding damage accumulation for zirconium alloys are given in (Semishkin, 2007) as

$$\dot{p}_e = f(k_i, T, \sigma_e, \omega(\tau)), \quad (9)$$

$$\dot{\omega}(\tau) = \frac{\sigma_e \cdot \dot{p}_e}{A_0}, \quad (10)$$

where  $k_i$  are material parameters defined from experiments with micromodels cut out along the FE cladding orthotropy directions;  $T$  is absolute temperature, K.

According to (Semishkin, 2007), for LOCA-accidents only, using the failure condition  $\omega(\tau) = 1$ , the SDE value  $A_0$  accumulated by the moment of cladding failure and supposed to be temperature-dependent only, is determined from the equations (9)-(10). At the same time, the assumption that the value of  $A_0$  at high-temperature creep and cladding failure analysis is loading history independent, is accepted for LOCA-accidents as an experimentally proved matter.

In contrast to the experimental technique for determining  $A_0$  developed in (Semishkin, 2007), the calculation method proposed in (Pelykh et al., 2008) means that  $A_0$  can be found by any of two ways:

1. As the SDE value at the moment  $\tau_0$  of cladding stability loss, which is determined by condition  $\sigma_e^{\max}(\tau_0) = \sigma_0^{\max}(\tau_0)$ , when equivalent stress  $\sigma_e^{\max}(\tau)$  becomes equal to yield stress  $\sigma_0^{\max}(\tau)$  for the point of the cladding having the maximum temperature (according to the calculation model, a fuel rod is divided into axial and radial segments).
2. As the SDE value at the rapid creep start moment for the cladding point having the maximum temperature. This way is the most conservative approach, and it is not obvious that such level of conservatism is really necessary when estimating  $A_0$ .

The equivalent stress  $\sigma_e$  and the rate of equivalent creep strain  $\dot{p}_e$  are calculated by the LWR fuel analysis code FEMAXI (Suzuki, 2000). Though cladding creep test data must have been used to develop and validate the constitutive models used in the finite element code FEMAXI to calculate the equivalent creep strains under cyclic loading, difficulty of this problem is explained by the fact that cladding material creep modeling under the conditions corresponding to real operational variable load modes is inconvenient or impossible as such tests can last for years. As a rule, the real FE operational conditions can be simulated in such tests very approximately only, not taking into account all the variety of possible exploitation situations (Semishkin, 2007).

The code FEMAXI analyzes changes in the thermal, mechanical and chemical state of a single fuel rod and interaction of its components in a given NR power history and coolant



conditions. The code analytical scope covers normal operation conditions and transient conditions such as load-following and rapid power increase in a high-burnup region of over 50 MWd/kg-U.

In the creep model used in the code, irradiation creep effects are taken into consideration and rate of equivalent cladding creep strain  $\dot{p}_e$  is expressed with a function of cladding stress, temperature and fast neutron flux (MATPRO-09, 1976):

$$\dot{p}_e = K \cdot \Phi (\sigma_\theta + B \cdot \exp(C \cdot \sigma_\theta)) \exp(-Q / R \cdot T) \tau^{-0.5}, \quad (11)$$

where  $\dot{p}_e$  is biaxial creep strain rate,  $s^{-1}$ ;  $K$ ,  $B$ ,  $C$  are known constants characterizing the cladding material properties;  $\Phi$  is fast neutron flux ( $E > 1.0$  MeV),  $1/m^2 \cdot s$ ;  $\sigma_\theta$  is circumferential stress, Pa;  $Q = 10^4$  J/mol;  $R = 1.987$  cal/mol·K;  $T$  is cladding temperature, K;  $\tau$  is time, s.

According to (11), creep strain increases as fast neutron flux, cladding temperature, stress and irradiation time increase.

For creep under uniaxial stress, cladding and pellet creep equations can be represented as (Suzuki, 2010):

$$\dot{p}_e = f(\sigma_e, \varepsilon^H, T, \Phi, \dot{F}), \quad (12)$$

where  $\dot{p}_e$  is equivalent creep strain rate,  $c^{-1}$ ;  $\sigma_e$  is equivalent stress, Pa;  $\varepsilon^H$  is creep hardening parameter;  $\dot{F}$  is fission rate,  $1/m^3 \cdot s$ .

When equation (12) is generalized for a multi-axial stress state, the creep strain rate vector  $\{\dot{p}\}$  is expressed as a vector function  $\{\beta\}$  of stress and creep hardening parameter:

$$\{\dot{p}\} = \{\beta(\{\sigma\}, \varepsilon^H)\}, \quad (13)$$

where  $T$ ,  $\Phi$  and  $\dot{F}$  are omitted because they can be dealt with as known parameters.

When a calculation at time  $t_n$  is finished and a calculation in the next time increment  $\Delta t_{n+1}$  is being performed, the creep strain increment vector is represented as

$$\{\Delta p_{n+1}\} = \Delta t_{n+1} \{\dot{p}_{n+\theta}\} = \{\beta(\{\sigma_{n+\theta}\}, \varepsilon_{n+\theta}^H)\}, \quad (14)$$

where  $\{\sigma_{n+\theta}\} = (1 - \theta) \cdot \{\sigma_n\} + \theta \cdot \{\sigma_{n+1}\}$ ;  $\varepsilon_{n+\theta}^H = (1 - \theta) \cdot \varepsilon_n^H + \theta \cdot \varepsilon_{n+1}^H$ ;  $0 \leq \theta \leq 1$ .

In order to stress importance of numerical solution stability,  $\theta = 1$  is set.

Then, when the  $(i+1)$ -th iteration by the Newton-Raphson method is being performed after completion of the  $(i)$ -th iteration, the creep strain rate vector is expressed (Suzuki, 2010).

As shown in Fig. 1, the analysis model includes a 2-dimensional axisymmetrical system in which the entire length of a fuel rod is divided into AS, and each AS is further divided into concentric ring elements in the radial direction.

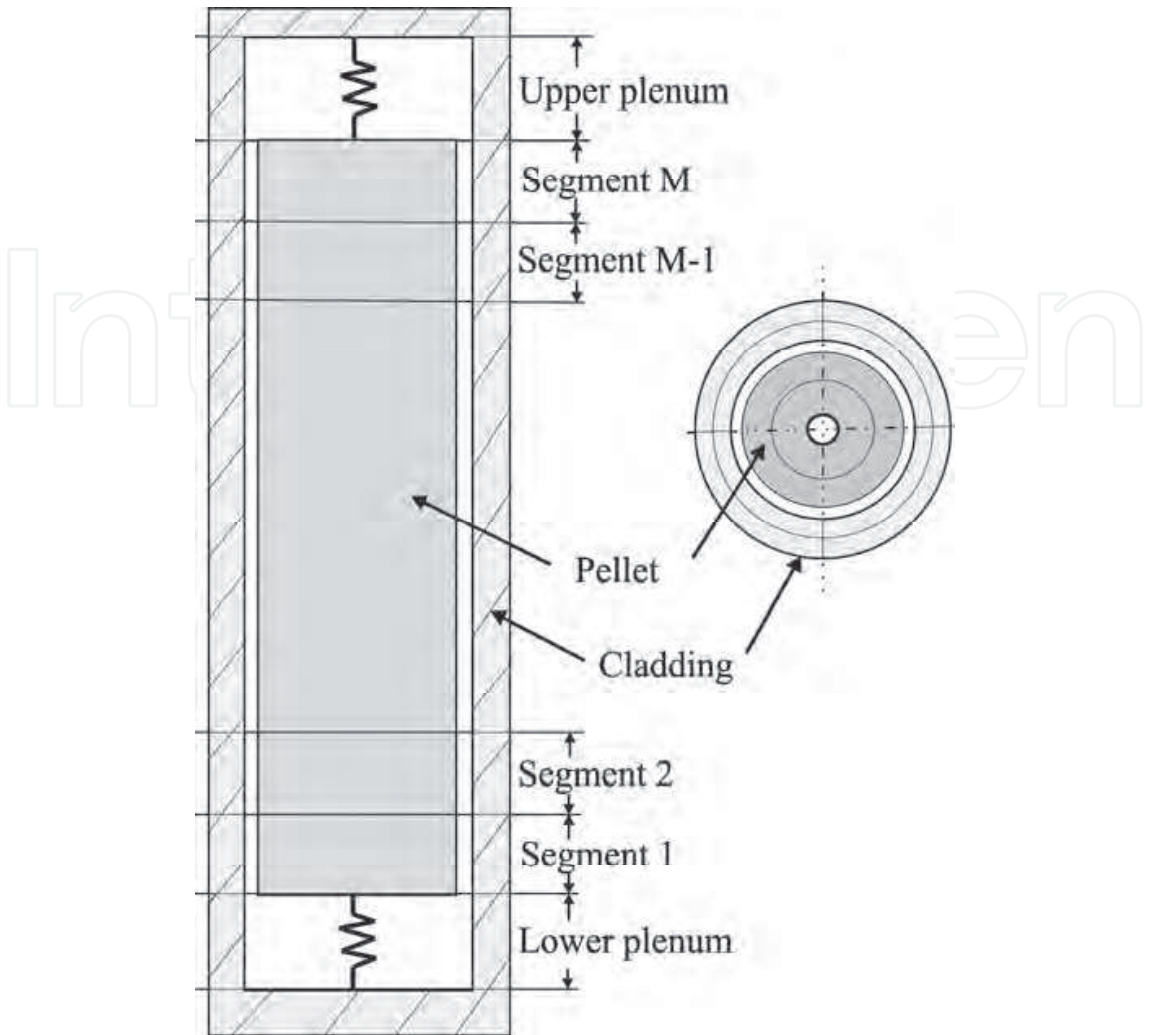


Fig. 1. Analysis model.

In this system, stress/strain analysis is performed using FEM with quadrangular elements having four degrees of freedom, as is shown in Fig. 2.

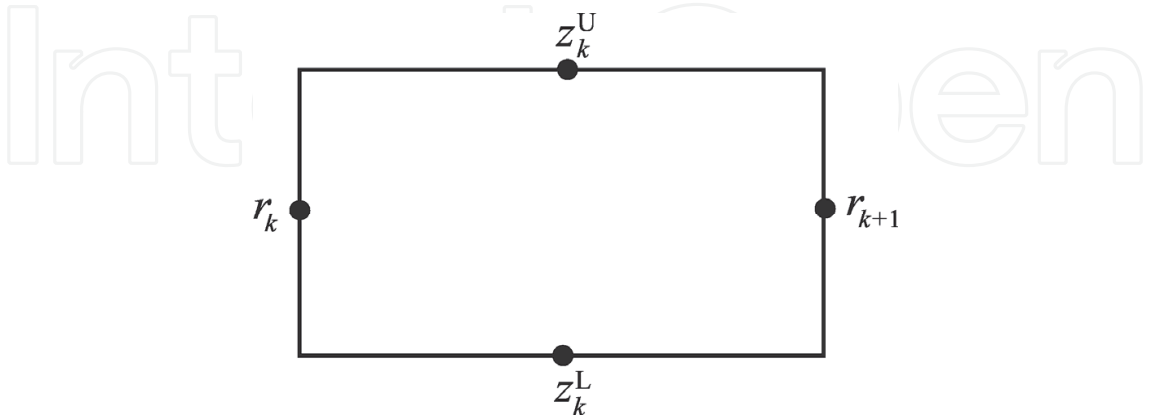


Fig. 2. Quadrangular model element with four degrees of freedom.

Fig. 3 shows relationship between mesh division and degree of freedom for each node in an AS.

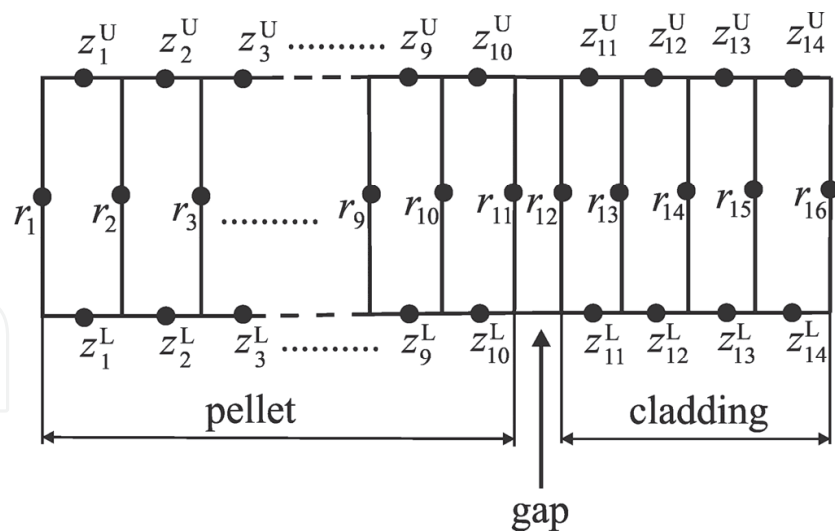


Fig. 3. Mesh division of FEM (for one AS).

In Fig. 3, the number of mesh divisions in the radial direction of pellet and cladding is fixed at 10 and 4, respectively. The inner two meshes of a cladding (11, 12) are metal phase, and the outer two meshes (13, 14) are oxide layer ( $\text{ZrO}_2$ ). The model used in the code takes into account that the oxide layer mesh and metal mesh are re-meshed and change their thickness with the progress of corrosion.

The fuel temperature calculation was carried out with the difference between the numerical solution and analytical solution not exceeding 0.1 %. The numerical error arising in the form of residue from iterative creep calculation on each time step, was not estimated as in most cases this error is exceeded by other uncertainties, first of all by thermal conductivity model error (Suzuki, 2010).

Denoting the number of daily load NR power cycles as  $N$ , using the CET-model, the dependence  $A(N)$ , as well as the borders of characteristic creep stages (unsteady, steady and rapid creep) for zircaloy cladding were obtained for the WWER daily load cycle (16 h – 100 %; 6 h –  $k \cdot 100$  %), where  $k = 1; 0.75; 0.5; 0.25$ . Hence the number of daily cycles  $N_{e,0}$  that the cladding can withstand prior to the rapid creep stage beginning could be calculated. The conclusion was made that the calculated value of  $A_0$  is not constant for a given material and depends on the operating mode of multiple cyclic power changes (Pelykh, 2008).

It was found, that the calculated equivalent creep strain  $p_e$  for zircaloy cladding, for all daily load modes, gradually increases and a hysteresis decrease of  $p_e$  can be seen at the last creep stage beginning. Then, after the hysteresis decrease,  $p_e$  starts to grow fast and achieves considerable values from cladding reliability point of view. At the rapid creep beginning, the equivalent stress  $\sigma_e$  decrease trend changes into the  $\sigma_e$  increase trend, at the same time  $p_e$  decreases a little, that is there is a “hysteresis loop”, when the  $p_e$  increase has got a phase delay in comparison with the  $\sigma_e$  increase. It should be noted, that the cause of the  $p_e$  hysteresis decrease effect must be additionally studied as  $p_e$  is expected to continuously increase unless the cladding is subjected to significant compressive creep stresses during the cycle and that this had been properly included in the creep material model.

The following new NR power daily maneuver algorithm was proposed in (Maksimov et al., 2009). It is considered that a nuclear unit is working at the nominal power level (100 %),

unwanted xenon oscillations are suppressed by the NR control group movement. At first, boric acid solution is injected so that the NR capacity decreases to 90 %, while the NR inlet coolant temperature is maintained constant at the expense of the Main Steam Line (MSL) pressure rise. To guarantee suppression of xenon oscillations, the optimal instantaneous Axial Offset (AO) is maintained due to the NR control group movement. Further the NR power is lowered at the expense of poisoning. The NR capacity will reach the 80% level in 2–3 h and the capacity will be stabilized by intake of the “pure distillate”. The NR capacity will be partly restored at the expense of depoisoning starting after the maximal iodine poisoning. To restore the nominal NR power level, the “pure distillate” is injected into the NR circuit and the MSL pressure is lowered, while the NR coolant inlet temperature is maintained constant. The optimal instantaneous AO to be maintained, the control rod group is extracted from the active core. The automatic controller maintains the capacity and xenon oscillations are suppressed by the control group movement after the NR has reached the nominal power level.

The proposed algorithm advantages: lowering of switching number; lowering of “pure distillate” and boric acid solution rate; lowering of unbalanced water flow; improvement of fuel operation conditions. Also, the proposed NR capacity program meaning the NR inlet coolant temperature stability, while the MSL pressure lies within the limits of 5.8–6.0 MPa and the NR capacity changes within the limits of 100–80 %, has the advantages of the well known capacity program with the first circuit coolant average temperature constancy.

The capacity program with the first circuit coolant average temperature constancy is widely used at Russian nuclear power units with WWER-reactors due to the main advantage of this program consisting of the possibility to change the unit power level when the reactor control rods stay at almost constant position. At the same time, as the MSL pressure lies within the procedural limits, the proposed algorithm is free of the constant first circuit temperature program main disadvantage consisting of the wide range of MSL pressure change. Two WWER-1000 daily maneuver algorithms were compared in the interests of efficiency (Maksimov et al., 2009):

1. The algorithm tested at KhNPP (“Tested”) on April 18, 2006: power lowering to 80 % within 1 h – operation at the 80 % power level within 7 h – power rising to 100 % within 2 h.
2. The proposed algorithm (“Proposed”): power lowering to 90 % by boric acid solution injection within 0.5 h – further power lowering to 80 % at the expense of NR poisoning within 2.5 h – operation at the 80 % power level within 4 h – power rising to 100 % within 2 h.

Comparison of the above mentioned daily maneuver algorithms was done with the help of the “Reactor Simulator” (RS) code (Philimonov and Mamichev, 1998). To determine axial power irregularity, AO is calculated as

$$AO = \frac{N_u - N_l}{N},$$

where  $N_u$ ,  $N_l$ ,  $N$  are the core upper half power, lower half power and whole power, respectively.

The instantaneous AO corresponds to the current xenon distribution, while the equilibrium AO corresponds to the equilibrium xenon distribution. Having used the proposed method

of cladding failure estimation for zircaloy cladding and WWER-type NR, dependence of the irreversible creep deformation accumulated energy from the number of daily load cycles is calculated for the “Tested” and “Proposed” algorithms, and efficiency comparison is fulfilled – see Table 3.

Algorithm	Easy of NR power field stabilization		CF	The number of daily cycles $N_{e,0}$ that cladding can withstand prior to the rapid creep beginning, eff. days
	Divergency of instantaneous and equilibrium AO diagrams	Amplitude of AO change during the maneuver		
“Tested”	considerable divergency	considerable amplitude	0.929	705
“Proposed”	slight divergency	amplitude is more than 10 times less	0.942	706

Table 3. Efficiency comparison for two daily maneuvering algorithms.

For the “Proposed” algorithm, taking into account the lower switching number necessary to enter “pure distillate” and boric acid solution during the maneuver, slight divergency of the instantaneous and equilibrium AO diagrams, the lower amplitude of AO change during the maneuver, the higher turbo-generator efficiency corresponding to the higher CF, as well as in consideration of practically equal cladding operation times for both the algorithms, it was concluded that the “Proposed” algorithm was preferable (Maksimov et al., 2009).

Using this approach, the complex criterion of power maneuvering algorithm efficiency for WWER-1000 operating in the mode of variable loading, taking into account FE cladding damage level, active core power stability, NR capacity factor, as well as control system reliability, has been worked out (Pelykh et al., 2009). Also the Compromise-combined WWER-1000 power control method capable of maximum variable loading operation efficiency, has been proposed and grounded (Maksimov and Pelykh, 2010).

3. Factors influencing durability of WWER FE cladding under normal conditions

Using the CET cladding durability estimation method, an analysis of the cladding (stress relieved zircaloy) durability estimation sensitivity to the WWER-1000 main regime and design initial data uncertainty, under variable loading conditions, has been done. The WWER-1000 main regime and design parameters have been divided into two groups: the parameters that influence the cladding failure conditions slightly and the parameters that determine the cladding failure conditions. The second group includes such initial parameters that any one of them gives a change of  $\tau_0$  estimation near 2 % (or greater) if the initial parameter has been specified at the value assignment interval of 3 %. This group consists of outer cladding diameter, pellet diameter, pellet hole diameter, cladding thickness, pellet



effective density, maximum FE linear heat rate, coolant inlet temperature, coolant inlet pressure, coolant velocity, initial He pressure, FE grid spacing, etc. (Maksimov and Pelykh, 2009). For example, dependence of cladding SDE on the number of effective days  $N$ , for pellet centre hole diameter  $d_{hole} = 0.140$  cm, 0.112 cm and 0.168 cm, is shown in Fig. 4.

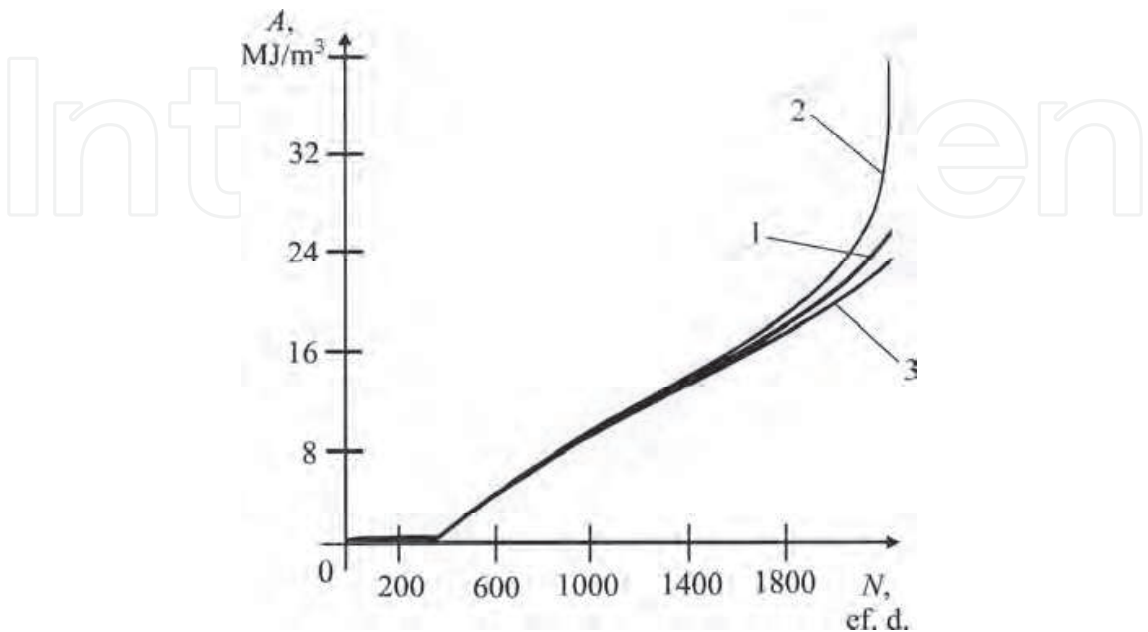


Fig. 4. Dependence of SDE on  $N$  for  $d_{hole}$ : 0.140 cm (1); 0.112 cm (2); 0.168 cm (3).

Dependence of cladding equivalent stress  $\sigma_e^{\max}(\tau)$  and yield stress  $\sigma_0^{\max}(\tau)$ , for the cladding point having the maximum temperature, on the number of effective days  $N$ , for  $d_{hole} = 0.112$  cm and 0.168 cm, is shown in Fig. 5.

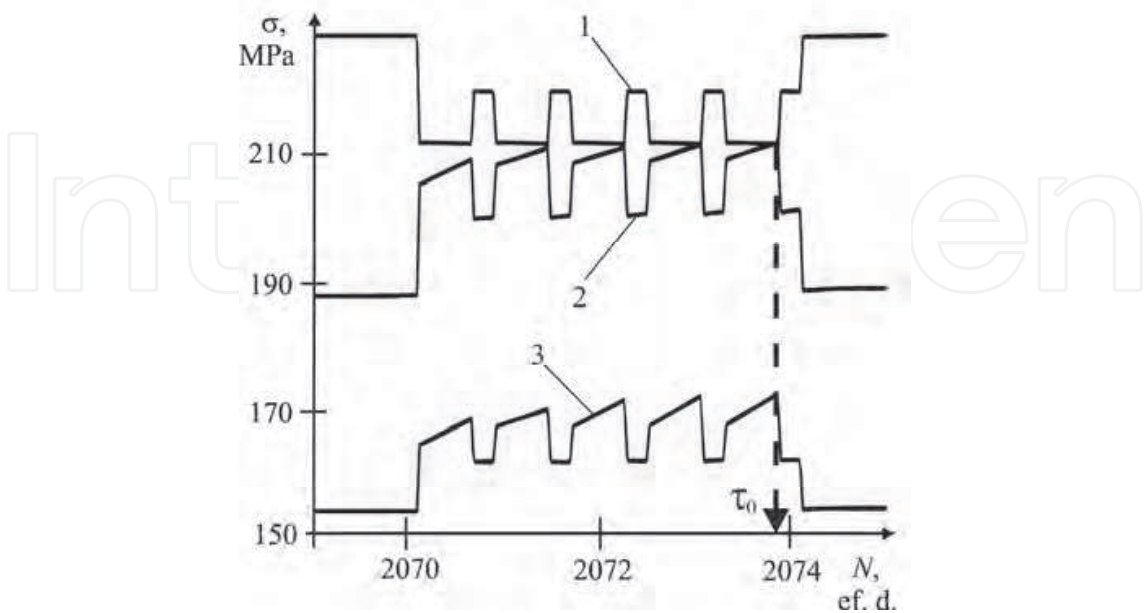


Fig. 5. Dependence of cladding yield stress (1) and equivalent stress (2; 3) on  $N$  for  $d_{hole}$ : 0.112 cm (2); 0.168 cm (3). Determination of  $\tau_0$  for  $d_{hole} = 0.112$  cm.



Using the value of  $\tau_0$  and the calculated dependence of SDE on  $N$ , the value of  $A_0$  is found – see Fig. 6.

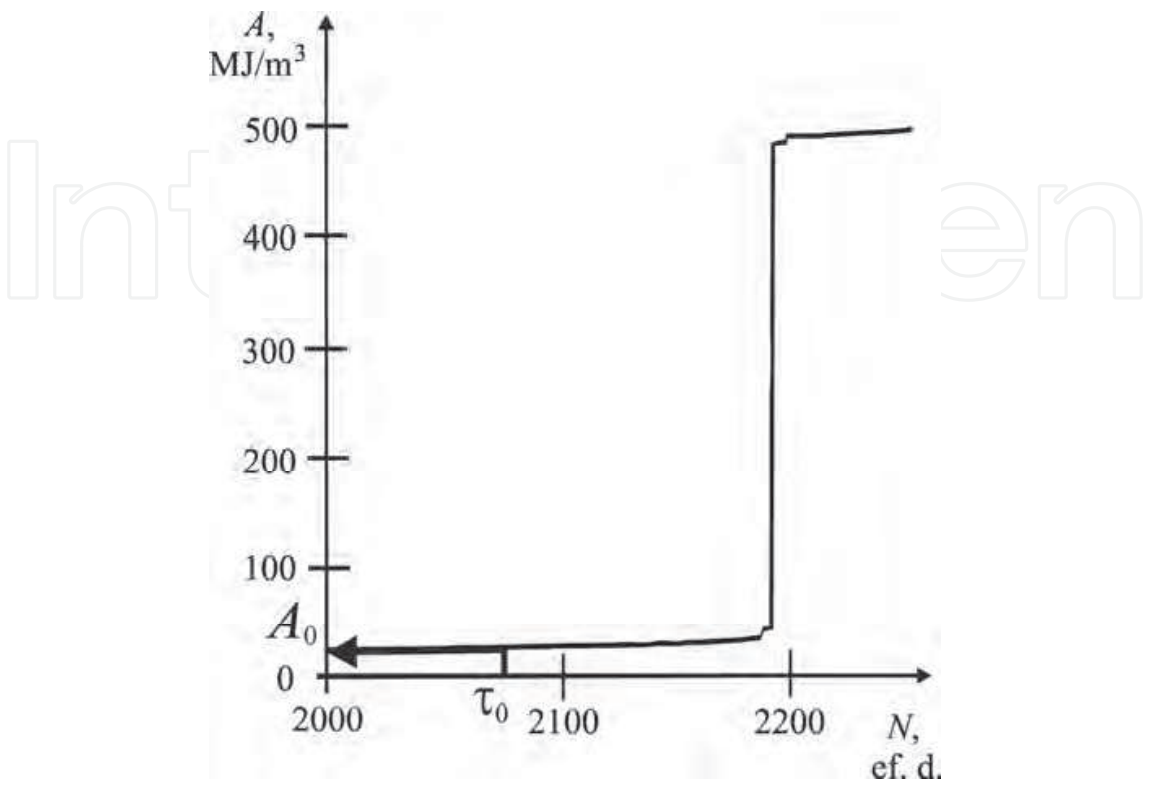


Fig. 6. Calculation of  $A_0$ .

For the combined variable load cycle, dependence of cladding SDE on the number of effective days  $N$  for a medium-loading FE of UTVS , TVS-A and TVS-W, is shown in Fig. 7.

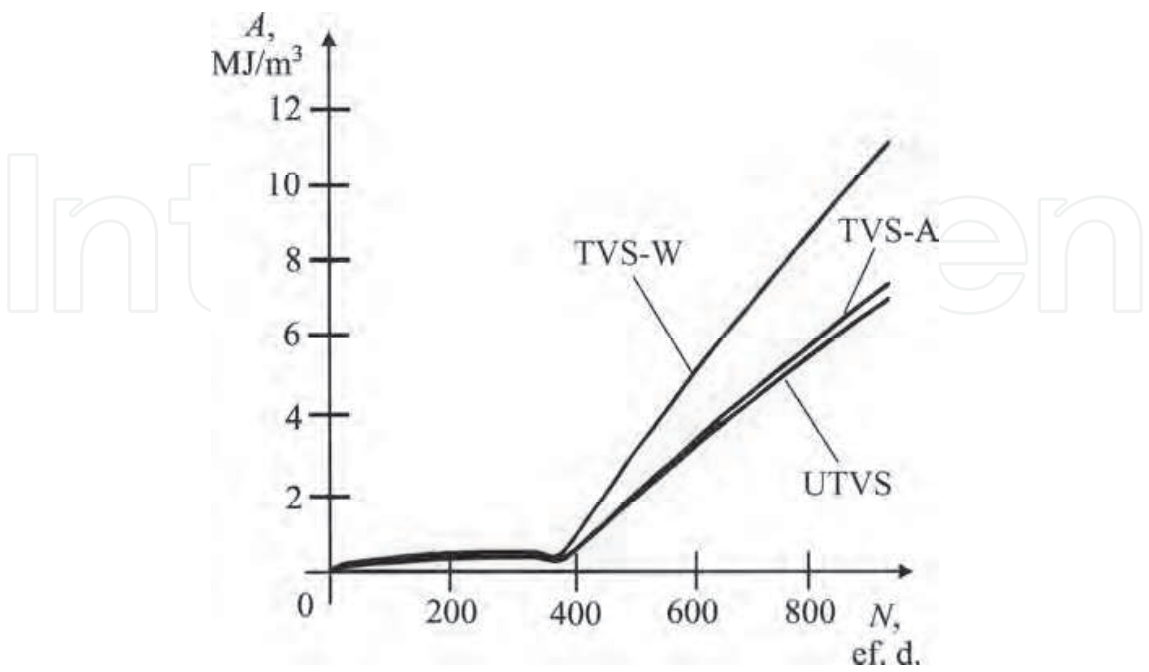


Fig. 7. Dependence of SDE on  $N$  for UTVS, TVS-A and TVS-W.

For the combined cycle, the maximum SDE value was obtained for a medium-loading FE of the FA produced by WESTINGHOUSE, which has no pellet centre hole (see Table 1). The same result was obtained for the stationary regime of WWER-1000 (Maksimov and Pelykh, 2010).

It has been found that cladding running time, expressed in cycles, for the WWER-1000 combined load cycle decreases from 1925 to 1351 cycles, when FE maximum LHR  $q_{l,max}$  increases from 248 W/cm to 298 W/cm (Maksimov and Pelykh, 2010). Having done estimation of cladding material failure parameter  $\omega$  after 1576 ef. days, it was found that the WWER-1000 combined load cycle has an advantage in comparison with stationary operation at 100 % power level when  $q_{l,max} \leq 273$  W/cm – see Table 4.

According to FEM, a FE length is divided into  $n$  equal length AS. In the first publications devoted to the CET-method it was supposed that the central AS is most strained and shortest-lived. However, this assumption does not consider that segments differ in LHR jump value. In addition, it was assumed that a FA stays in the same place over the whole fuel operating period (Maksimov and Pelykh, 2009).

Parameter	FE maximum LHR, W/cm				
	248	258	263	273	298
	Average fast neutron flux density, cm <sup>-2</sup> s <sup>-1</sup>				
	1 · 10 <sup>14</sup>	1.04 · 10 <sup>14</sup>	1.06 · 10 <sup>14</sup>	1.1 · 10 <sup>14</sup>	1.2 · 10 <sup>14</sup>
Stationary loading					
$\tau_0$ , ef. d.	2211	2078	2016	1904	1631
$A_0$ , MJ/m <sup>3</sup>	33.37	35.66	36.87	39.74	47.64
$\omega$ , %	60	65	68	74	94
Combined variable loading					
$\tau_0$ , ef. d.	2246	2102	2032	1903	1576
$A_0$ , MJ/m <sup>3</sup>	27.36	29.14	30.05	32.10	37.69
$\omega$ , %	57	64	67	74	100

Table 4. Cladding damage parameter for stationary loading and the combined variable loading of WWER-1000.

At last, influence of cladding corrosion rate on cladding durability at variable loading was not taken into account. Thus it is necessary to estimate influence of varying duty on all AS, to take account of a real FA transposition algorithm as well as to consider influence of cladding corrosion rate on its durability.

4. Method to determine the most strained cladding axial segment

The amplitude of LHR jumps in AS occurring when the NR thermal power capacity  $N$  increases from 80% to 100% level, was estimated by the instrumentality of the RS code, which is a verified tool of the WWER-1000 calculation modelling (Philimonov and Mamichev, 1998). Using the RS code, the WWER-1000 core neutron-physical calculation numerical algorithms are based on consideration of simultaneous two-group diffusion equations, which are solved for a three-dimensional object (the reactor core) composed of a limited number of meshes.

The amplitude of LHR jumps was calculated for the following daily power maneuvering method: lowering of  $N$  from  $N_1=100\%$  to  $N_2=90\%$  by injection of boric acid solution within 0.5 h – further lowering of  $N$  to  $N_3=80\%$  due to reactor poisoning within 2.5 h – operation at  $N_3=80\%$  within 4 h – rising of  $N$  to the nominal capacity level  $N_1=100\%$  within 2 h (Maksimov et al., 2009). According to this maneuvering method, the inlet coolant temperature is kept constant while the NR capacity changes in the range  $N=100\text{--}80\%$ , and the initial steam pressure of the secondary coolant circuit changes within the standard range of 58–60 bar. It was supposed that the only group of regulating units being used at NR power maneuvering was the tenth one, while the control rods of all the other groups of regulating units were completely removed from the active core. The next assumption was that the Advanced power control algorithm (A-algorithm) was used. The WWER-1000 core contains ten groups of regulating units in case of the A-algorithm – see Fig. 8.

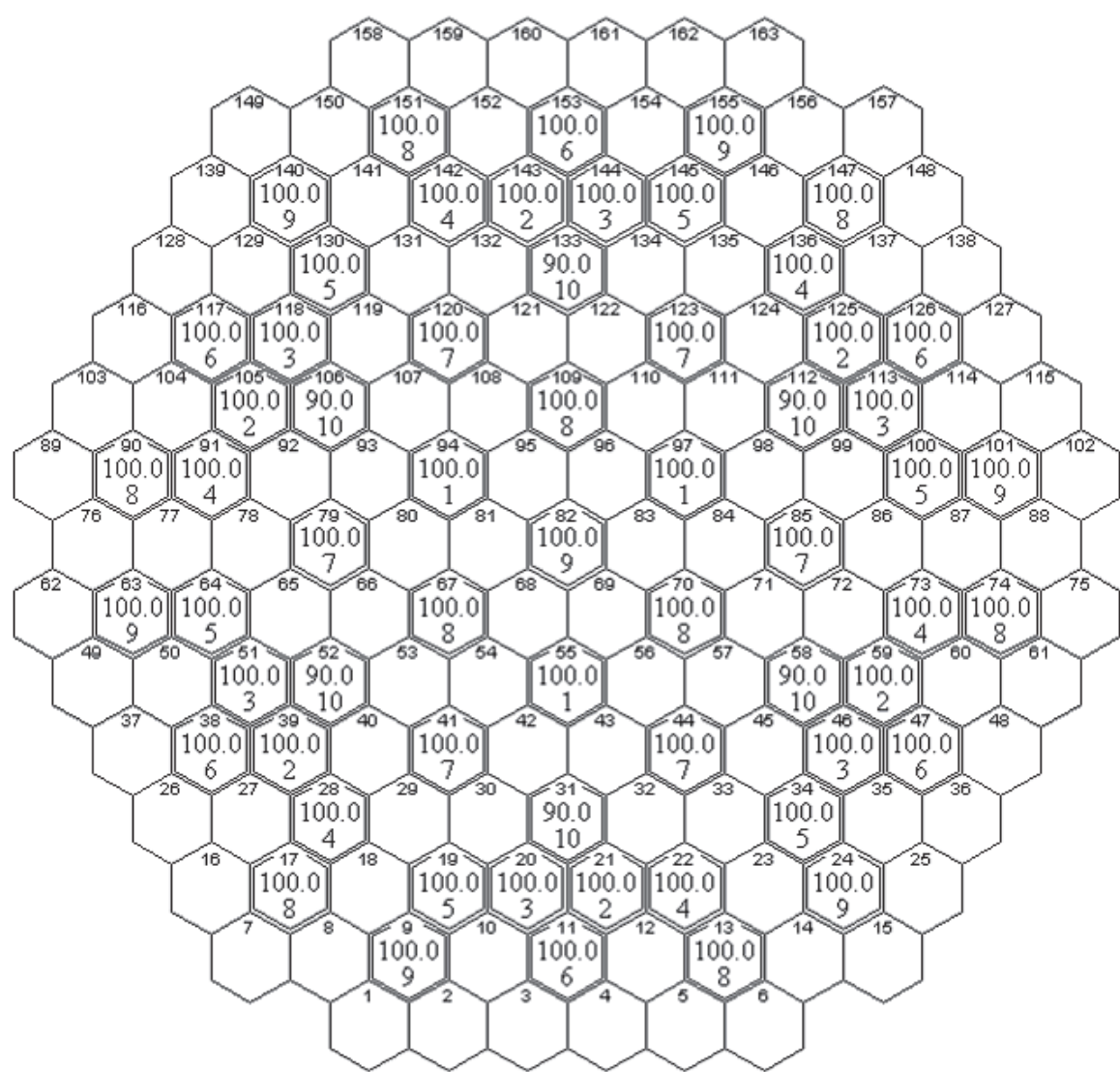


Fig. 8. Disposition of the WWER-1000 regulating units in case of the A-algorithm: (upper figure) the FA number; (middle figure) the lowest control rod axial coordinate (at 100% NR power level) measured from the core bottom, %; (lower figure) the regulating unit group number.

The lowest control rod axial coordinates for  $N_1=100\%$  and  $N_3=80\%$  were designated  $H_1=90\%$  and  $H_3=84\%$ , respectively. That is when  $N$  changes from  $N_1=100\%$  to  $N_3=80\%$ , the lowest control rod axial coordinate measured from the core bottom changes from  $H_1=90\%$  to  $H_3=84\%$ .

It has been found using the RS code that the WWER-1000 fuel assemblies can be classified into three groups by the FA power growth amplitude occurring when the NR capacity increases from 80% to 100% level – see Table 5 (Pelykh et al., 2010).

FA group	The number of fuel assemblies	FA power growth, %	FA numbers (according to the core cartogram )
1	6	28	31, 52, 58, 106, 112, 133
2	37	26	20, 42, 43, 46, 51, 53...57, 66...71, 80...84, 93...98, 107...111, 113, 118, 121, 122, 144
3	120	≤ 25	all other fuel assemblies

Table 5. Three groups of the WWER-1000 fuel assemblies.

When the eighth, ninth and tenth regulating groups are simultaneously used, the central FA (No. 82) as well as fresh fuel assemblies are regulated by control rods. But when using the A-algorithm, the tenth regulating group is used only. In this case, such a four-year FA transposition algorithm can be considered as an example: a FA stays in the 55-th FA (FE maximum LHR  $q_l^{\max} = 236.8$  W/cm, FA group 2) position for the first year – then the FA stays in the 31-st FA ( $q_l^{\max} = 250.3$  W/cm, group 1) position for the second year – further the FA stays in the 69-th FA ( $q_l^{\max} = 171.9$  W/cm, group 2) position for the third year – at last, the FA stays in the central 82-d FA ( $q_l^{\max} = 119.6$  W/cm, group 2) position for the fourth year (the algorithm 55–31–69–82).

The average LHR for  $i$ -segment and  $j$ -FA is denoted as  $\langle q_{l,i,j} \rangle$ . For all segments ( $n = 8$ ) of the 55-th, 31-st, 69-th and 82-nd fuel assemblies, the values of  $\langle q_{l,i,j} \rangle$  have been calculated at power levels of  $N_3=80\%$  and  $N_1=100\%$  using the RS code. The  $\langle q_{l,i,j} \rangle (100\%) / \langle q_{l,i,j} \rangle (80\%)$  ratio values are listed in Table 6.

AS	FA number			
	55	31	69	82
8	1.341	1.517	1.328	1.340
7	1.308	1.426	1.297	1.309
6	1.250	1.241	1.263	1.268
5	1.229	1.213	1.238	1.250
4	1.224	1.217	1.232	1.242
3	1.241	1.229	1.243	1.259
2	1.255	1.251	1.271	1.270
1	1.278	1.275	1.288	1.302

Table 6. The  $\langle q_{l,i,j} \rangle (100\%) / \langle q_{l,i,j} \rangle (80\%)$  ratio values for fuel assemblies 55, 31, 69, 82.

Though the Nb-containing zirconium alloy E-110 (Zr + 1% Nb) has been used for many years in FE of WWER-1000, there is no public data on E-110 cladding corrosion and creep rates for all possible loading conditions of WWER-1000. In order to apply the cladding durability estimation method based on the corrosion and creep models developed for Zircaloy-4 to another cladding alloy used in WWER-1000, it is enough to prove that using these models under the WWER-1000 active core conditions ensures conservatism of the E-110 cladding durability estimation. Nevertheless, the main results of the present analysis will not be changed by including models developed for another cladding alloy.

The modified cladding failure criterion at NR variable loading is given as (Pelykh and Maksimov, 2011):

$$\omega(\tau) = A(\tau) / A_0 = 1; A(\tau) = \int_0^\tau \sigma_e^{\max}(\tau) \dot{p}_e^{\max}(\tau) d\tau; A_0 \text{ at } \sigma_e^{\max}(\tau_0) = \eta \sigma_0^{\max}(\tau_0), \tag{15}$$

where  $\omega(\tau)$  is cladding material failure parameter;  $\tau$  is time, s;  $A(\tau)$  is SDE, J/m<sup>3</sup>;  $A_0$  is SDE at the moment  $\tau_0$  of cladding material failure beginning, when  $\sigma_e^{\max}(\tau_0) = \eta \sigma_0^{\max}(\tau_0)$ ;  $\sigma_e^{\max}(\tau)$  and  $\dot{p}_e^{\max}(\tau)$  are equivalent stress (Pa) and rate of equivalent creep strain (s<sup>-1</sup>) for the cladding point of an AS having the maximum temperature, respectively;  $\sigma_0^{\max}(\tau)$  is yield stress for the cladding point of an AS having the maximum temperature, Pa;  $\eta$  is some factor,  $\eta \leq 1$ .

Assuming the 55-31-69-82 four-year FA transposition algorithm and  $\eta = 0.6$ , the  $\omega(\tau)$  values have been calculated by Eq. (15) using the following procedure: calculating  $\sigma_e^{\max}(\tau)$ ,  $\dot{p}_e^{\max}(\tau)$  and  $\sigma_0^{\max}(\tau)$  by the instrumentality of FEMAXI-V code (Suzuki, 2000); calculating  $A(\tau)$ ; determining the moment  $\tau_0$  according to the condition  $\sigma_e^{\max}(\tau_0) = \eta \sigma_0^{\max}(\tau_0)$ ; determining  $A_0 \equiv A(\tau_0)$ ; calculating  $\omega(\tau)$  - see Table 7 (Pelykh and Maksimov, 2011).

$\tau$ , days	AS			
	4	5	6	7
360	0.063	0.151	0.190	0.175
720	0.598	0.645	0.647	0.547
1080	0.733	0.783	0.790	0.707
1440	0.788	0.838	0.848	0.779

Table 7. Cladding failure parameters  $\omega(\tau)$  for the axial segments 4-7.

For the other axial segments No. 1-3 and 8, on condition that a FA was transposed in concordance with the 55-31-69-82 four-year algorithm, the  $\omega(\tau)$  value was less than 1.0, i.e. there was no cladding collapse up to  $\tau = 2495$  days. For  $\tau > 2495$  days calculations were not carried out. For all the axial segments, on condition that a FA was transposed in concordance with the 55-31-69-82 four-year algorithm, it has been found that there was no cladding collapse up to  $\tau = 2495$  days with  $\omega(\tau) = 1$ . At the same time, for all the axial segments, on condition that a FA stayed in the 55-th FA position for all fuel operation period, as well as on condition that a FA stayed in the 55-th FA position for the first year,



then it stayed in the 31-st FA position for the remaining fuel operation period, the  $\omega(\tau)$  value reached 1.0 and the cladding collapse was predicted at  $\tau < 2495$  days with  $\eta = 1$ .

The prediction shown in Table 7 that the largest value of  $\omega(\tau)$  exists at the fifth (central) axial segment and above it the value drops in the sixth segment situated between the axial coordinates  $z = 2.19$  and  $2.63$  m reflects the fact that the most considerable LHR jumps take place at the core upper region (see Table 6). Thus, taking account of the 55–31–69–82 four-year FA transposition algorithm as well as considering the regulating unit disposition, on condition that the FE length is divided into eight equal-length axial segments, the sixth (counting from the core bottom) AS cladding durability limits the WWER-1000 operation time at daily cycle power maneuvering.

Growth of the water-side oxide layer of cladding can cause overshoot of permissible limits for the layer outer surface temperature prior to the cladding collapse moment. The corrosion models of EPRI (MATPRO-09, 1976) and MATPRO-A (SCDAP/RELAP5/MOD2, 1990) have been used for zircaloy cladding corrosion rate estimation. According to the EPRI model, the cladding corrosion rate for a bubble flow is estimated as

$$dS / dt = (A / S^2) \exp(-Q_1 / R T_b) (1 + \text{COR}), \quad (16)$$

where  $dS / dt$  is the oxide growth rate,  $\mu\text{m}/\text{day}$ ;  $A = 6.3 \times 10^9 \mu\text{m}^3/\text{day}$ ;  $S$  is the oxide layer thickness,  $\mu\text{m}$ ;  $Q_1 = 32289 \text{ cal/mol}$ ;  $R = 1.987 \text{ cal/(mol K)}$ ;  $T_b$  is the temperature at the oxide layer-metal phase boundary, K; COR is an adjusting factor which is added in the FEMAXI code (Suzuki, 2010).

According to the MATPRO-A model, the oxide layer thickness for a nucleate boiling flow is estimated as

$$S = (4.976 \times 10^{-3} A t \exp(-15660 / T_b) + S_0^3)^{1/3} (1 + \text{COR}), \quad (17)$$

where  $S$  is the oxide layer thickness, m;  $A = 1.5$  (PWR);  $t$  is time, days;  $T_b$  is the temperature at the oxide layer-metal phase boundary, K;  $S_0$  is the initial oxide layer thickness, m.

The cladding failure parameter values listed in Table 7 have been obtained using the MATPRO-A corrosion model at  $\text{COR} = 1$ . If COR is the same in both the models, the MATPRO-model estimation of cladding corrosion rate is more conservative than the EPRI-model estimation, under the WWER-1000 conditions. Regardless of the model we use, the factor COR must be determined so that the calculated oxide layer thickness fits to experimental data. The oxide layer thickness calculation has been carried out for the described method of daily power maneuvering, assuming that a FA was transposed in concordance with the 55–31–69–82 four-year algorithm. The calculations assumed that, the Piling-Bedworth ratio was 1.56, the initial oxide layer thickness was  $0.1 \mu\text{m}$ , the maximum oxide layer thickness was restricted by  $100 \mu\text{m}$ , the radial portion of cladding corrosion volume expansion ratio was 80%. It has been found that the calculated cladding oxide layer thickness, for the WWER-1000 conditions and burnup  $Bu = 52.5 \text{ MW day/kg}$ , conforms to the generalized experimental data obtained for PWR in-pile conditions (Bull, 2005), when using the EPRI model at  $\text{COR} = -0.431$  – see Fig. 9.



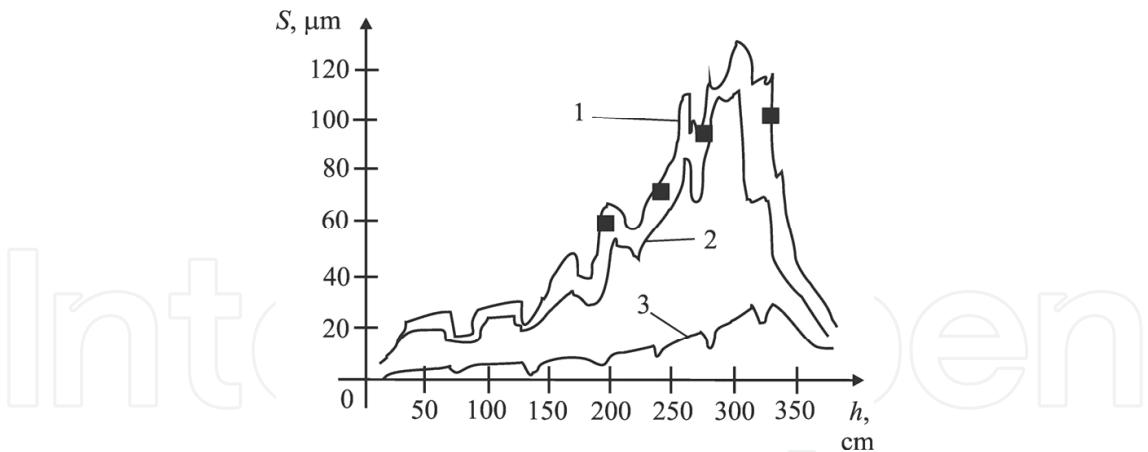


Fig. 9. Cladding oxide layer thickness  $S$  subject to height  $h$ : (■) calculated using the EPRI model at  $COR = -0.431$ ; In accordance with (Bull, 2005): (1) zircaloy-4; (2) improved zircaloy-4; (3) ZIRLO.

The EPRI model at  $COR = -0.431$  also gives the calculated cladding oxide layer thickness values which were in compliance with the generalized experimental data for zircaloy-4 (Kesterson and Yueh, 2006). For the segments 5–8, assuming that a FA was transposed in concordance with the 55–31–69–82 four-year algorithm, the maximum oxide layer outer surface temperature  $T_{ox,out}^{max}$  during the four-year fuel life-time has been calculated (EPRI,  $COR = -0.431$ ) – see Table 8. Also, for the segments 5–8, the calculated oxide layer thickness  $S$  and oxide layer outer surface temperature  $T_{ox,out}$  subject to time  $\tau$  are listed in Table 8.

The maximum oxide layer outer surface temperature during the four-year fuel life-time does not exceed the permissible limit temperature  $T_{ox,out}^{lim}=352\text{ }^{\circ}\text{C}$  (Shmelev et al., 2004).

i	$T_{ox,out}^{max},\text{ }^{\circ}\text{C}$	$S,\text{ }\mu\text{m} (T_{ox,out},\text{ }^{\circ}\text{C})$			
		360 days	720 days	1080 days	1440 days
5	345.1	11.3 (342.3)	40.6 (344.8)	58.1 (328.2)	69.8 (316.7)
6	349.6	16.1 (347.6)	49.8 (349.4)	69.3 (332.6)	82.5 (320.1)
7	351.2	18.1 (350.0)	52.7 (351.0)	74.1 (336.1)	88.5 (323.0)
8	348.0	14.2 (347.9)	38.3 (346.9)	58.0 (335.6)	71.2 (323.3)

Table 8. The maximum oxide layer outer surface temperature.

The same result has been obtained for the EPRI model at  $COR = 0; 1; 2$  as well as for the MATPRO-A model at  $COR = -0.431; 0; 1; 2$ . Hence the oxide layer outer surface temperature should not be considered as the limiting factor prior to the cladding collapse moment determined in accordance with the criterion (15). Though influence of the outer oxide layer thickness on the inner cladding surface temperature must be studied.

Having calculated the SDE by the instrumentality of FEMAXI (Suzuki, 2010), assuming that a FA was transposed in concordance with the 55–31–69–82 four-year algorithm, it has been found for the sixth axial segment that the number of calendar daily cycles prior to the beginning of the rapid creep stage was essentially different at  $COR = -0.431; 0; 1$ ; and 2. As a result, the rapid creep stage is degenerated for both the corrosion models at  $COR = -0.431$  (Fig. 10).

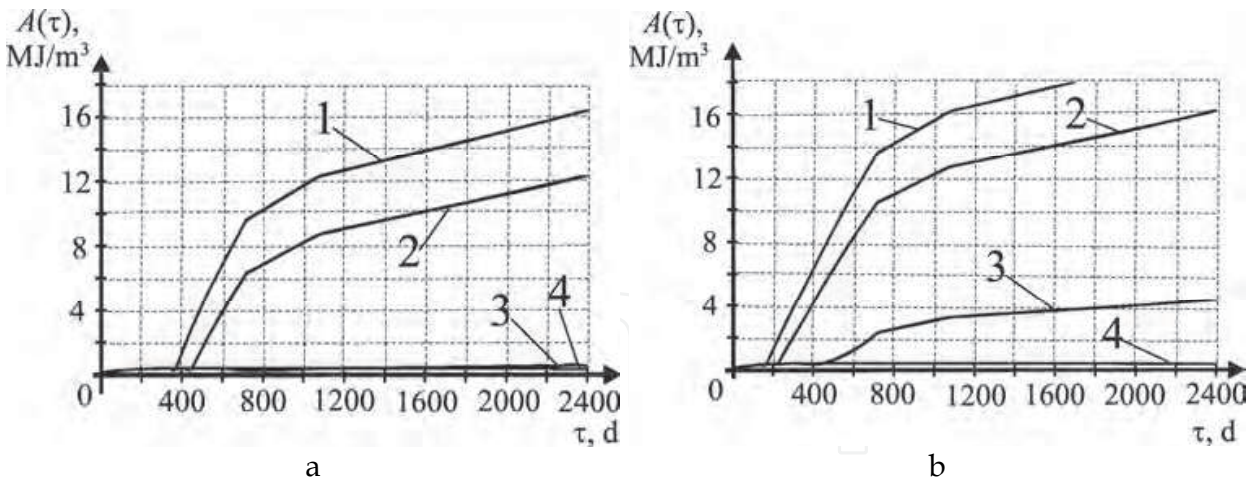


Fig. 10. The SDE as a function of time for the sixth axial segment:(1, 2, 3, 4) at COR = 2, 1, 0, -0.431, respectively; (a) the EPRI model corrosion; (b) the MATPRO-A model corrosion.

Let us introduce a dimensionless parameter  $I$

$$I = \frac{10^{-6}}{^{\circ}\text{C} \cdot \text{day}} \int_0^T T_{clad,in} \cdot dt, \tag{18}$$

where  $T_{clad,in}$  is the cladding inner surface temperature for an axial segment,  $^{\circ}\text{C}$ ; and  $t$  is time, days.

Having analysed the described method of daily power maneuvering, the maximum cladding oxide layer outer surface temperature  $T_{ox,out}^{\max}$  during the period of 2400 days, as well as  $I(2400 \text{ days})$  and the 2400 days period averaged cladding inner surface temperature  $\langle T_{clad,in} \rangle$  have been calculated for the sixth segment, using the EPRI corrosion model – see Table 9.

COR	$T_{ox,out}^{\max}, ^{\circ}\text{C}$	$I(2400 \text{ days})$	$\langle T_{clad,in} \rangle, ^{\circ}\text{C}$
2	349.2	0.951	396.2
1	349.5	0.947	394.5
0	349.6	0.938	390.7
-0.431	349.6	0.916	381.8

Table 9. Cladding temperatures subject to COR for the sixth segment, the EPRI model corrosion.

This shows that the effect of cladding outer surface corrosion rate (with COR) on the cladding SDE increase rate (see Fig. 10) is induced by the thermal resistance of oxide thickness and the increase in  $T_{clad,in}$  (see Table 9).

It should be noticed that the metal wall thickness decrease due to oxidation is considered in the calculation of the SDE, as effect of the cladding waterside corrosion on heat transfer and mechanical behavior of the cladding is taken into account in the FEMAXI code. Since

temperature and deformation distributions physically depend on each other, simultaneous equations of thermal conduction and mechanical deformation are solved (Suzuki, 2000).

It is obvious that the cladding temperature at the central point of an AS increases when the outer oxide layer thickness increases. At the same time, according to the creep model (MATPRO-09, 1976) used in the code, the rate of equivalent creep strain  $\dot{\epsilon}_e^{\max}(\tau)$  for the central point of an axial segment increases when the corresponding cladding temperature increases. Hence the waterside corrosion of cladding is associated with the evaluation of SDE through the creep rate depending on the thickness of metal wall (Pelykh and Maksimov, 2011).

It should be noted, that neutron irradiation has a great influence on the zircaloy corrosion behavior. Power maneuvering will alter neutron flux to give a feedback to the corrosion behavior, either positive or negative. But in this paper, the EPRI model and MATPRO code are used in the corrosion model, where irradiation term is not evidently shown. Although either temperature or reactivity coefficient is introduced in applying the model, it does not fully represent such situation.

For the studied conditions, the maximum cladding hoop stress, plastic strain and oxide layer outer surface temperature do not limit cladding durability according to the known restrictions  $\sigma_{\theta}^{\max} \leq 250 \text{ MPa}$ ,  $\epsilon_{\theta,pl}^{\max} \leq 0.5\%$  (Novikov et al., 2005) and  $T_{ox,out}^{\max} \leq 352 \text{ }^{\circ}\text{C}$  (Shmelev et al., 2004), respectively. A similar result has been obtained for the corrosion model MATPRO-A.

Setting COR = 0 and COR = 1 (MATPRO-A), the SDE values for the algorithms 55-31-55-55 and 55-31-69-82 have been calculated. Then the numbers of calendar daily cycles prior to the beginning of rapid creep stage for Zircaloy-4 (Pelykh and Maksimov, 2011) and rapid  $\omega(\tau)$  stage for E-110 alloy (Novikov et al., 2005) have been compared under WWER-1000 conditions – see Fig. 11.

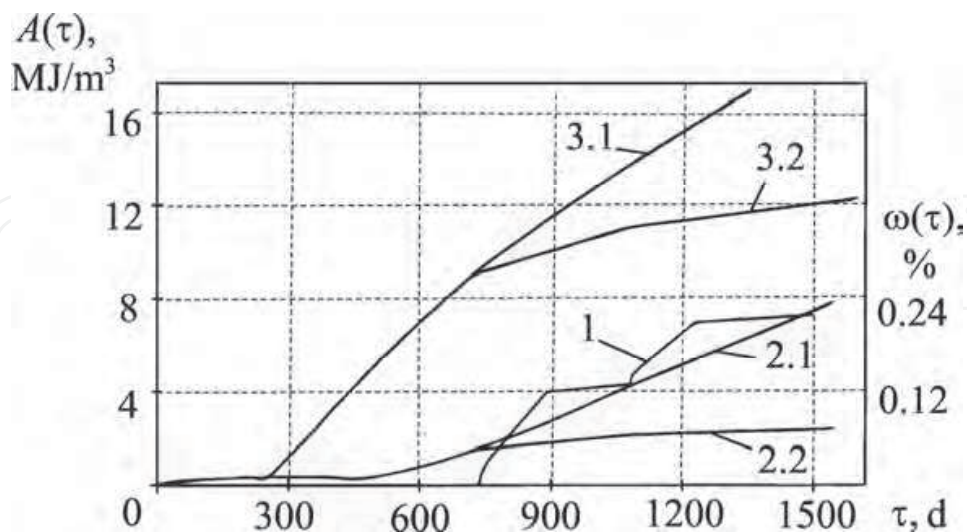


Fig. 11. Cladding damage parameter (E-110) and SDE (Zircaloy-4) as functions of time: (1)  $\omega(\tau)$  according to equation (2); (2.1, 2.2)  $A(\tau)$  at COR = 0 for the algorithms 55-31-55-55 and 55-31-69-82, respectively; (3.1, 3.2)  $A(\tau)$  at COR = 1 for the algorithms 55-31-55-55 and 55-31-69-82, respectively.

It is necessary to notice that line 1 in Fig. 11 was calculated using separate consideration of steady-state operation and varying duty. When using equation (2), the fatigue component has an overwhelming size in comparison with the static one (Novikov et al., 2005).

Use of the MATPRO-A corrosion model under the WWER-1000 core conditions ensures conservatism of the E-110 cladding durability estimation (see Fig. 11). Growth rate of  $A(\tau)$  depends significantly on the FA transposition algorithm. The number of daily cycles prior to the beginning of rapid creep stage decreases significantly when COR (cladding outer surface corrosion rate) increases.

Setting the WWER-1000 regime and FA constructional parameters, a calculation study of Zircaloy-4 cladding fatigue factor at variable load frequency  $\nu \ll 1$  Hz, under variable loading, was carried out. The investigated WWER-1000 fuel cladding had an outer diameter and thickness of 9.1 mm and 0.69 mm, respectively. The microstructure of Zircaloy-4 was a stress-relieved state. Using the cladding corrosion model EPRI (Suzuki, 2000), AS 6 of a medium-load FE in FA 55 (maximum LHR  $q_l^{\max} = 229.2$  W/cm at  $N = 100$  %) has been analysed (COR = 1, inlet coolant temperature  $T_{in} = \text{const} = 287$  °C). The variable loading cycle 100–80–100 % was studied for  $\Delta\tau = 11; 5; 2$  h (reactor capacity factor CF=0.9):  $N$  lowering from 100 to 80 % for 1 h  $\rightarrow$  exploitation at  $N = 80$  % for  $\Delta\tau$  h  $\rightarrow N$  rising to  $N_{nom} = 100$  % for 1 h  $\rightarrow$  exploitation at  $N = 100$  % for  $\Delta\tau$  h, corresponding to  $\nu = 1; 2; 4$  cycle/day, respectively ( $\nu \ll 1$  Hz).

Calculation of the cladding failure beginning moment  $\tau_0$  depending on  $\nu$  showed that if  $\nu \ll 1$  Hz and CF=idem, then there was no decrease of  $\tau_0$  after  $\nu$  had increased 4 times, in comparison with the case  $\nu = 1$  cycle/day, taking into account the estimated error  $< 0.4$  % ( $\eta = 0.4$ , AS 6). At the same time, when  $N = 100$  % =const (CF=1), the calculated  $\tau_0$  decreases significantly – see Table 10.

Hence, the WWER-1000 FE cladding durability estimation based on the CET model corresponds to the experimental results (Kim et al., 2007) in principle.

CF	0.9			1
$\nu$ , cycle/day	1	2	4	-
$\tau_0$ , day	547.6	547.0	549.0	436.6

Table 10. Change of cladding failure time depending on  $\nu$  and CF.

In the creep model used in the FEMAXI code (Suzuki, 2000), irradiation creep effects are taken into consideration and cladding creep strain rate  $\dot{p}_e(\tau)$  is expressed with a function of fast neutron flux, cladding temperature and hoop stress (MATPRO-09, 1976). Thus creep strain increases as fast neutron flux, irradiation time, cladding temperature and stress increase. Fast neutron flux is predominant in cladding creep rate, whereas thermal neutron distribution is a determining factor for reactivity and thermal power (temperature of cladding) in core. It can be seen that both types of neutron flux are important for the cladding life.

One of main tasks at power maneuvering is non-admission of axial power flux xenon waves in the active core. Therefore, for a power-cycling WWER-1000 nuclear unit, it is interesting to consider a cladding rupture life control method on the basis of stabilization of neutron flux axial distribution. The well-known WWER-1000 power control method based on keeping the average coolant temperature constant has such advantages as most favorable conditions for the primary coolant circuit equipment operation, as well as possibility of stable NR power regulation due to the temperature coefficient of reactivity. However, this method has such defect as an essential raise of the secondary circuit steam pressure at power lowering, which requires designing of steam generators able to work at an increased pressure.

Following from this, it is an actual task to develop advanced power maneuvering methods for the ENERGOATOM WWER-1000 units which have such features as neutron field axial distribution stability, favorable operation conditions for the primary circuit equipment, especially for FE claddings, as well as avoidance of a high pressure steam generator design. The described daily power maneuvering method with a constant inlet coolant temperature allows to keep the secondary circuit initial steam pressure within the standard range of 58-60 bar ( $N=100-80\%$ ).

The nonstationary reactor poisoning adds a positive feedback to any neutron flux deviation. Therefore, as influence of the coolant temperature coefficient of reactivity is a fast effect, while poisoning is a slow effect having the same sign as the neutron flux deviation due to this reactivity effect, and strengthening it due to the positive feedback, it can be expected that a correct selection of the coolant temperature regime ensures the neutron flux density axial distribution stability at power maneuvering. The neutron flux axial stability is characterized by AO (Philipchuk et al., 1981):

$$AO = \frac{N_u - N_l}{N}, \quad (19)$$

where  $N_u$ ,  $N_l$ ,  $N$  are the core upper half power, lower half power and whole power, respectively.

The variables  $AO$ ,  $N_u$ ,  $N_l$ ,  $N$  are represented as

$$AO = AO_0 + \delta AO; N_u = N_{u,0} + \delta N_u; N_l = N_{l,0} + \delta N_l; N = N_0 + \delta N, \quad (20)$$

where  $AO_0$ ,  $N_{u,0}$ ,  $N_{l,0}$ ,  $N_0$  are the stationary values of  $AO$ ,  $N_u$ ,  $N_l$ ,  $N$ , respectively;  $\delta AO$ ,  $\delta N_u$ ,  $\delta N_l$ ,  $\delta N$  are the sufficiently small deviations from  $AO_0$ ,  $N_{u,0}$ ,  $N_{l,0}$ ,  $N_0$ , respectively.

The small deviations of  $N_u$  and  $N_l$  caused by the relevant average coolant temperature deviations  $\delta \langle T_u \rangle$  and  $\delta \langle T_l \rangle$  are expressed as

$$\delta N_u = \frac{\delta N}{\delta \langle T \rangle} \cdot \delta \langle T_u \rangle; \delta N_l = \frac{\delta N}{\delta \langle T \rangle} \cdot \delta \langle T_l \rangle, \quad (21)$$

where  $\delta N_u$  and  $\delta N_l$  are the small deviations of  $N_u$  and  $N_l$ , respectively;  $\delta \langle T \rangle$  is the average coolant temperature small deviation for the whole core;  $\delta \langle T_u \rangle$  and  $\delta \langle T_l \rangle$  are the



average coolant temperature small deviations for the upper half-core and for the lower half-core, respectively.

The term  $\delta N / \delta \langle T \rangle$  is expressed as

$$\frac{\delta N}{\delta \langle T \rangle} = \frac{\delta \rho / \delta \langle T \rangle}{\delta \rho / \delta N} \equiv \frac{k_T}{k_N}, \quad (22)$$

where  $\rho$  is reactivity;  $k_T$  and  $k_N$  are the coolant temperature coefficient of reactivity and the power coefficient of reactivity, respectively.

Having substituted equations (20)–(22) in (19), the following equation for a small deviation of AO caused by a small deviation of  $N$  is derived after linearization:

$$\delta AO = \frac{k_T}{k_N} \cdot N_0^{-1} \cdot [(1 - AO_0) \cdot \delta \langle T_u \rangle - (1 + AO_0) \cdot \delta \langle T_l \rangle] \quad (23)$$

In case of the assumption

$$AO_0 \ll 1 \quad (24)$$

equation (23) is simplified:

$$\delta AO = \frac{k_T}{k_N} \cdot N_0^{-1} \cdot [\delta \langle T_u \rangle - \delta \langle T_l \rangle] \quad (25)$$

The criterion of AO stabilization due to the coolant temperature coefficient of reactivity (the coolant temperature regime effectiveness criterion) is obtained from (25):

$$\min \left| \sum_{i=1}^m [\delta \langle T_u \rangle - \delta \langle T_l \rangle] \right|, \quad (26)$$

where  $i$  is the power step number;  $m$  is the total number of power steps in some direction at reactor power maneuvering.

Use of the criterion (26) allows us to select a coolant temperature regime giving the maximum LHR axial distribution stability at power maneuvering. Let us study the following three WWER-1000 power maneuvering methods: M-1 is the method with a constant inlet coolant temperature  $T_{in} = \text{const}$ ; M-2 is the method with a constant average coolant temperature  $\langle T \rangle = \text{const}$ ; and M-3 is the intermediate method having  $T_{in}$  increased by 1 °C only, when  $N$  lowers from 100% to 80%. Comparison of these power maneuvering methods has been made using the RS code. Distribution of long-lived and stable fission products causing reactor slagging was specified for the KhNPP Unit 2 fifth campaign start, thus the first core state having an equilibrium xenon distribution was calculated at this moment. The non-equilibrium xenon and samarium distributions were calculated for subsequent states taking into account the fuel burnup. The coolant inlet pressure and coolant flow rate were specified constant and equal to 16 MPa and  $84 \cdot 10^3 \text{ m}^3/\text{h}$ , respectively. When using M-1, the coolant inlet temperature was specified at  $T_{in} = 287 \text{ °C}$ . When using M-



2, the coolant inlet temperature was specified according to Table 11 ( $T_{out}$  is the coolant outlet temperature).

$N, \%$	$T_{in}, \text{ }^{\circ}\text{C}$	$T_{out}, \text{ }^{\circ}\text{C}$	$\langle T \rangle, \text{ }^{\circ}\text{C}$
100	287	317	302
90	288	316	302
80	290	314	302

Table 11. Change of the coolant temperature at  $\langle T \rangle = \text{const}$  in the M-2 method.

Denoting change of the lowest control rod axial coordinate (%) measured from the core bottom during a power maneuvering as  $\Delta H$ , the first (M-2-a) and second (M-2-b) variants of M-2 had the regulating group movement amplitudes  $\Delta H_{2a} = 4\%$  and  $\Delta H_{2b} = 6\%$ , respectively. The reactor power change subject to time was set according to the same time profile for all the methods (Fig. 12).

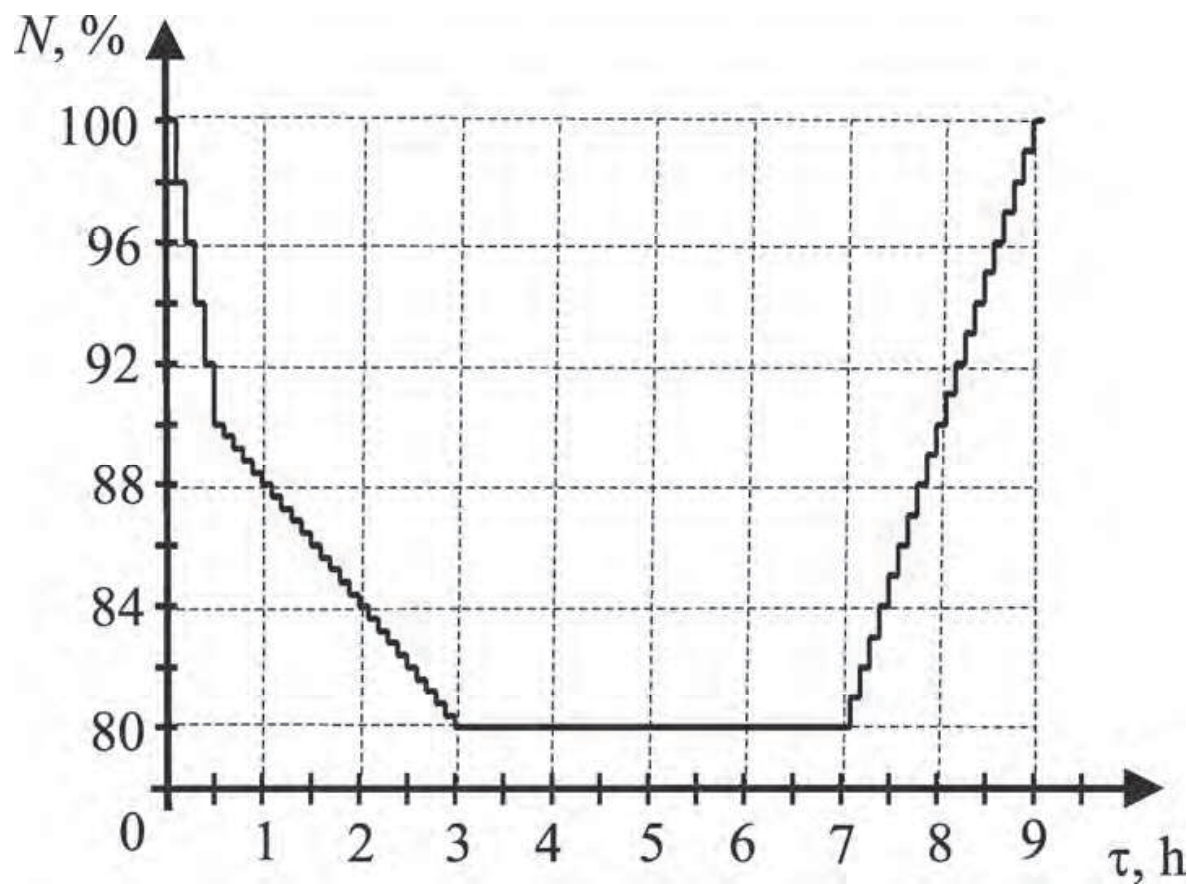


Fig. 12. Change of the reactor power subject to time.

For all the methods,  $N$  lowered from  $N_1 = 100\%$  to  $N_2 = 90\%$  within  $0.5\text{ h}$ , under the linear law  $dN_{1-2}/d\tau = -2\%/6\text{ min}$ , at the expense of boric acid entering. Also for all the methods,  $N$

lowered from  $N_2=90\%$  to  $N_3=80\%$  within 2.5 h, under the law  $dN_{2-3}/d\tau = -0.4\%/6 \text{ min}$ , at the expense of reactor poisoning. The coolant concentration of boric acid was the criticality parameter when  $N$  stayed constant during 4 h. The NR power increased from  $N_3=80\%$  to  $N_1=100\%$  within 2 h, under the law  $dN_{3-1}/d\tau = 1.0\%/6 \text{ min}$ , at the expense of pure distillate water entering and synchronous return of the regulating group to the scheduled position. When  $N$  increased from  $N_3=80\%$  to  $N_1=100\%$ , change of the regulating group position  $H$  subject to time was set under the linear law (Fig. 13).

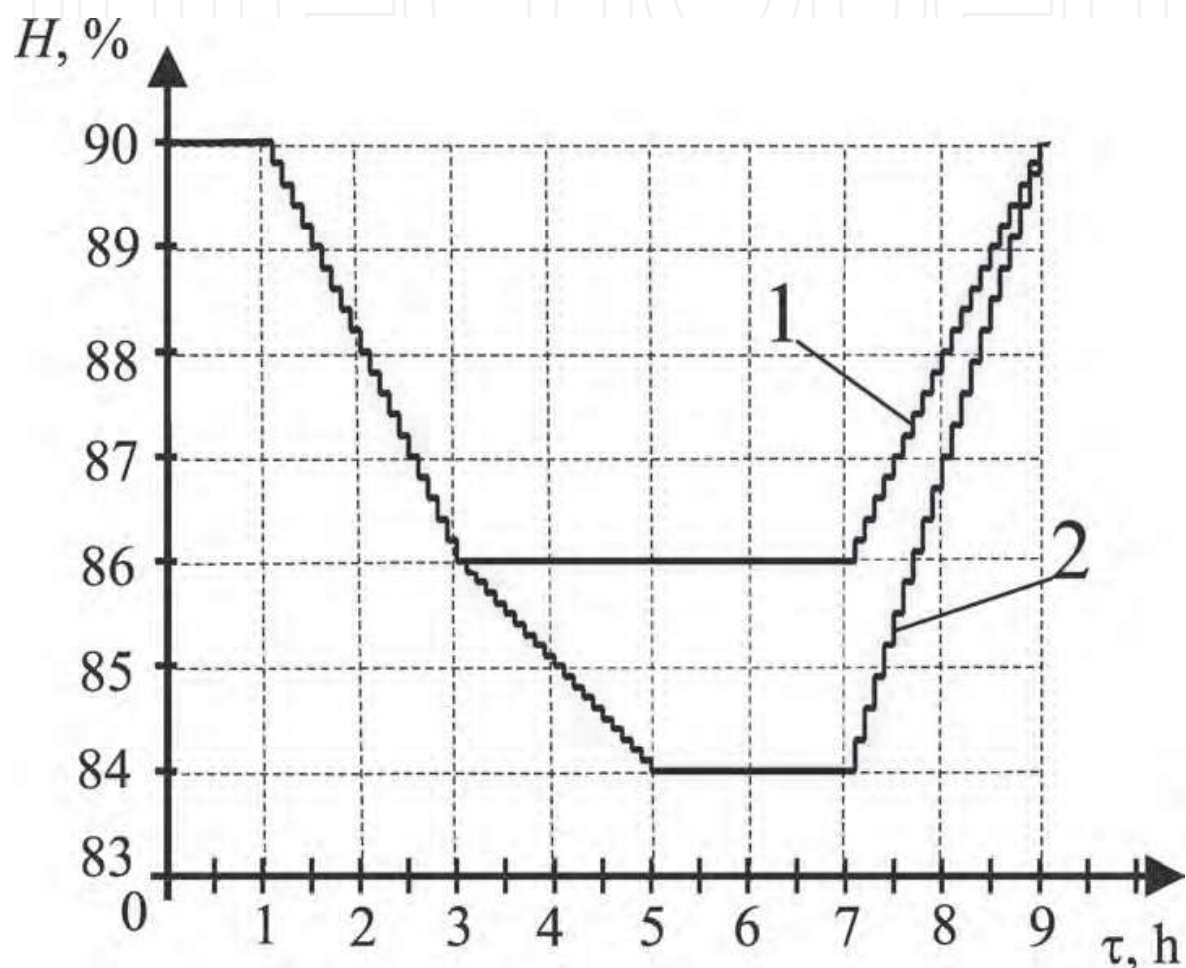


Fig. 13. Change of the regulating group position subject to time: (1) the methods M-1, M-2-a and M-3; (2) the method M-2-b.

Thus, modelling of the non-equilibrium WWER-1000 control was made by assignment of the following control parameters: criticality parameter;  $T_{in,0}$  ;  $dT_{in}/dN$ ;  $N_1$ ;  $N_2$ ;  $N_3$ ;  $H_0$ ;  $\Delta H$ ;  $dN/d\tau$ . Setting the WWER-1000 operation parameters in accordance with the Shmelev's method (Shmelev et al., 2004), for the methods M-1, M-2-a, M-2-b and M-3, when  $N$  changed from 100% to 80%, the change of core average LHR distribution was calculated by the RS code. Let us enter the simplifying representation

$$\Delta\delta T \equiv \delta < T_u > - \delta < T_l > \tag{27}$$

Using the obtained LHR distribution, by the FEMAXI code (Suzuki, 2010), the average coolant temperatures of the upper  $\langle T_u \rangle$  and lower  $\langle T_l \rangle$  half-cores were calculated for M-1, M-2-a and M-3 (at time step 0.5 h). Then, on the basis of  $\langle T_u \rangle$  and  $\langle T_l \rangle$ ,  $\left| \sum_{i=1}^6 \Delta \delta T \right|$  was found for M-1, M-2-a and M-3 having the same  $\Delta H$  (Table 12).

Method	$\tau, \text{h}$	$N, \%$	$\langle T_u \rangle$	$\langle T_l \rangle$	$\delta \langle T_u \rangle$	$\delta \langle T_l \rangle$	$\Delta \delta T$	$\left  \sum_{i=1}^6 \Delta \delta T \right $
M-1; M-2-a; M-3	0.1	100	318.3	296.825	0	0	0	2.65
M-1	0.6	90	317.975	296.575	-0.325	-0.25	-0.075	
	1.1	88	316.375	296	-1.6	-0.575	-1.025	
	1.6	86	315.725	295.725	-0.65	-0.275	-0.375	
	2.1	84	315.1	295.525	-0.625	-0.2	-0.425	
	2.6	82	314.5	295.3	-0.6	-0.225	-0.375	
	3.1	80	313.9	295.075	-0.6	-0.225	-0.375	
M-2-a	0.6	90	319.25	298.025	0.95	1.2	-0.25	2.85
	1.1	88	317.875	297.575	-1.375	-0.45	-0.925	
	1.6	86	317.45	297.575	-0.425	0	-0.425	
	2.1	84	316.925	297.575	-0.525	0	-0.525	
	2.6	82	316.65	297.625	-0.275	0.05	-0.325	
	3.1	80	316.35	297.725	-0.3	0.1	-0.4	
M-3	0.6	90	318.4	297.075	0.1	0.25	-0.15	2.70
	1.1	88	316.9	296.55	-1.5	-0.525	-0.975	
	1.6	86	316.35	296.4	-0.55	-0.15	-0.4	
	2.1	84	315.7	296.2	-0.65	-0.2	-0.45	
	2.6	82	315.225	296.125	-0.475	-0.075	-0.4	
	3.1	80	314.775	296	-0.45	-0.125	-0.325	

Table 12. Change of the average coolant temperatures for M-1, M-2-a, M-3.

Having used the criterion (26), the conclusion follows that the coolant temperature regime M-1 ensures the most stable AO, while the regime M-2-a is least favorable – see Table 12. In order to check this conclusion, it is useful to compare AO stabilization for the discussed methods, calculating the divergence  $\Delta \text{AO}$  between the instant and equilibrium axial offsets (Philimonov and Mamichev, 1998) – see Fig. 14.

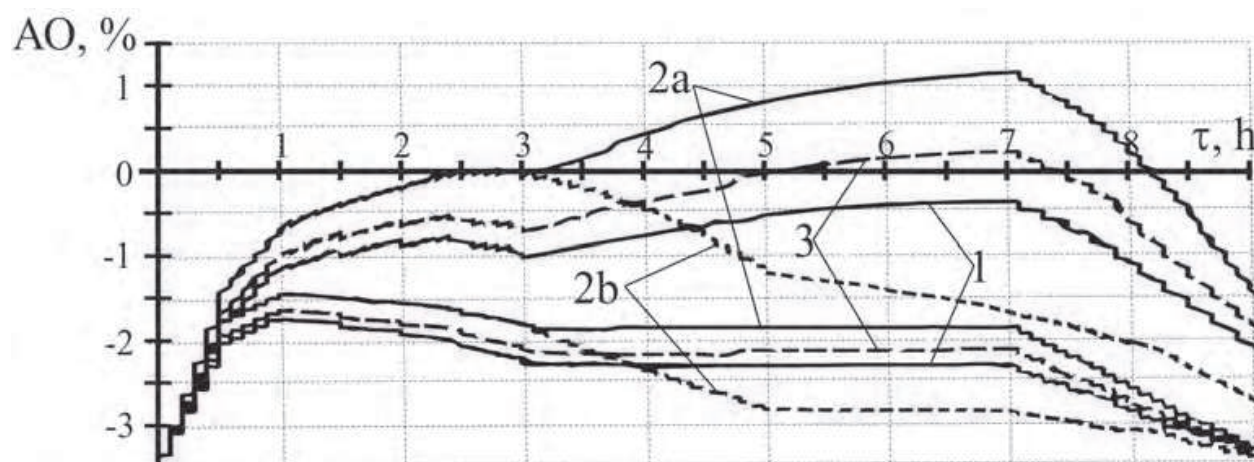


Fig. 14. Equilibrium and instant axial offsets (1, 2a, 2b, 3) subject to time for M-1, M-2-a, M-2-b and M-3, respectively: (lower line) the equilibrium AO; (upper line) the instant AO.

The regulating group movement amplitude is the same (4%) for M-1, M-2-a and M-3, but the maximum divergence between the instant and equilibrium offsets are  $\Delta AO_1^{\max} \approx 1.9\%$  (M-1),  $\Delta AO_{2a}^{\max} \approx 3\%$  (M-2-a) and  $\Delta AO_3^{\max} \approx 2.3\%$  (M-3). This result confirms the conclusion made on the basis of the criterion (26). If the regulating group movement amplitude, at power maneuvering according to the method with a constant average coolant temperature, is increased from 4 to 6%, then the maximum AO divergence lowers from 3% to 1.9% (see Fig. 14). Therefore, when using the method with  $\langle T \rangle = \text{const}$ , a greater regulating group movement amplitude is needed to guarantee the LHR axial stability, than when using the method with  $T_{in} = \text{const}$ , on the assumption that all other conditions for both the methods are identical.

Having used the RS code, the core average LHR axial distribution change has been calculated for the methods M-1, M-2-a, M-2-b and M-3, for the following daily power maneuvering cycle: lowering of  $N$  from  $N_1=100\%$  to  $N_2=90\%$  during 0.5 h by injection of boric acid solution – further lowering of  $N$  to  $N_3=80\%$  during 2.5 h due to reactor poisoning – operation at  $N_3=80\%$  during 4 h – rising of  $N$  to the nominal capacity level  $N_1=100\%$  during 2 h at the expense of pure distillate water entering and synchronous return of the regulating group to the scheduled position – operation at  $N_1=100\%$  during 15 h.

When using the criterion (15) for comparative analysis of cladding durability subject to the FA transposition algorithm, the position of an axial segment and the power maneuvering method, the value of  $\eta$  should be set taking into account the necessity of determining the moment  $\tau_0$ , when the condition  $\sigma_e^{\max}(\tau_0) = \eta \sigma_0^{\max}(\tau_0)$  is satisfied. In addition, as the maximum number of power history points is limited by  $n_p^{\lim} = 10,000$  in the FEMAXI code, the choice of  $\eta$  depends on the analysed time period  $\tau^{\max}$  and the complexity of a power maneuvering method, because a greater time period as well as a more complicated power maneuvering method are described by a greater number of history points  $n_p$ . Therefore, the value of  $\eta$  should be specified on the basis of simultaneous conditions  $\sigma_e^{\max}(\tau_0) = \eta \sigma_0^{\max}(\tau_0)$ ;  $n_p < n_p^{\lim}$ ;  $\tau_0 \leq \tau^{\max}$ . Though the cladding failure parameter values



listed in Table 6 were obtained assuming  $\eta = 0.6$  (the MATPRO-A corrosion model, COR = 1), comparison of cladding failure parameters for different power maneuvering methods can be made using the cladding collapse criterion (15), for instance, at  $\eta = 0.4$ . Assuming  $\eta = 0.4$ , on the basis of the obtained LHR distributions, the cladding failure parameters have been calculated by the instrumentality of the FEMAXI code (Suzuki, 2000) for the methods M-1, M-2-a, M-2-b and M-3, for the axial segments six and seven (the MATPRO-A corrosion model, COR = 1) – see Table 13.

Method		M-1	M-2-a	M-2-b	M-3
Axial Segment	$\tau_0$ , days	504.4	497.4	496.0	501.4
	6				
	$A_0$ , MJ / m <sup>3</sup>	1.061	1.094	1.080	1.068
	$\omega$ (500 days)	0.957	1.027 (+7.3%)	1.040 (+ 8.7%)	0.988 (+3.2%)
	$\tau_0$ , days	530.0	519.4	519.0	525.0
	7				
	$A_0$ , MJ / m <sup>3</sup>	1.044	1.055	1.019	1.043
	$\omega$ (500 days)	0.766	0.848 (+10.7%)	0.848 (+10.7%)	0.804 (+5.0%)

Table 13. Cladding failure parameters for the methods M-1, M-2-a, M-2-b and M-3.

Among the regimes with the regulating group movement amplitude  $\Delta H = 4\%$ , the coolant temperature regime M-1 ensuring the most stable AO is also characterized by the least calculated cladding failure parameter  $\omega$ (500 days) , while the regime M-2-a having the least stable AO is also characterized by the greatest  $\omega$ (500 days) – see Table 12, Fig. 14 and Table 13. The intermediate method M-3 having  $T_{in}$  increased by 1 °C only, when  $N$  lowers from 100% to 80%, is also characterized by the intermediate values of AO stability and  $\omega$ (500 days) .

In addition, the second variant of M-2 (M-2-b) having the regulating group movement amplitude  $\Delta H_{2b} = 6\%$  is characterized by a more stable AO in comparison with the method M-2-a (see Fig. 14) and, for the most strained axial segment six, by a greater value of  $\omega$ (500 days) – see Table 13.

It should be stressed that the proposed cladding rupture life control methods are not limited only in WWER-1000. Using the FEMAXI code, these methods can be extended into other reactor types (like PWR or BWR). At the same time, taking into account a real disposition of regulating units, a real coolant temperature regime as well as a real FA transposition algorithm, in order to estimate the amplitude of LHR jumps at FE axial segments occurring when the NR (PWR or BWR) capacity periodically increases, it is necessary to use another code instead of the RS code, which was developed for the WWER-1000 reactors.

The FA transposition algorithm 55-31-69-82 is characterized by a lower fuel cladding equivalent creep strain than the algorithm 55-31-55-55. At the same time, it has a lower fuel burnup than the algorithm 55-31-55-55 (see Table 14).

FA transposition algorithm	55-31-69-82		55-31-55-55	
COR	0	1	0	1
$B_U$ , MW·day/kg	57.4		71.4	
$\sigma_e^{\max}$ , MPa (% of $\sigma_0$ )	69.9 (33)	127.4 (61)	107.2 (51)	146.7 (70)
$p_e$ , %	4.22	11.22	9.36	16.02

Table 14. Fuel burnup and cladding equivalent creep strain for AS 6 (after 1500 d).

Thus, an optimal FA transposition algorithm must be set on the basis of cladding durability-fuel burnup compromise.

5. Methods of fuel cladding durability control at NPP with WWER

As is shown, the operating reactor power history as well as the WWER-1000 main regime and design parameters included into the second conditional group (pellet hole diameter, cladding thickness, pellet effective density, maximum FE linear heat rate, etc.) influence significantly on fuel cladding durability. At normal operation conditions, the WWER-1000 cladding corrosion rate is determined by design constraints for cladding and coolant, and depends slightly on the regime of variable loading. Also the WWER-1000 FE cladding rupture life, at normal variable loading operation conditions, depends greatly on the coolant temperature regime and the FA transposition algorithm. In addition, choice of the group of regulating units being used at NR power maneuvering influences greatly on the offset stabilization efficiency (Philimonov and Mamichev, 1998).

Hence, under normal operation conditions, the following methods of fuel cladding durability control at NPP with WWER can be considered as main ones:

- choice of the group of regulating units being used at power maneuvering.
- balance of stationary and variable loading regimes;
- choice of FE construction and fuel physical properties, e.g., for the most strained AS, making the fuel pellets with centre holes;
- assignment of the coolant temperature regime;
- assignment of the FA transposition algorithm;

To create a computer-based fuel life control system at NPP with WWER, it is necessary to calculate the nominal and maximum permissible values of pick-off signals on the basis of calculated FA normal operation probability (Philipchuk et al., 1981). Though a computer-based control system SAKOR-M has already been developed for NPP with WWER at the OKB “Gidropress” (Bogachev et al., 2007), this system does not control the remaining life of fuel assemblies.

As the described CET-method can be applied to any type of LWR including prospective thorium reactors, the future fuel life control system for NPP with LWR can be created using this physically based method.



## 6. Conclusions

Taking into account the WWER-1000 fuel assembly four-year operating period transposition algorithm, as well as considering the disposition of control rods, it has been obtained that the axial segment, located between  $z = 2.19$  m and  $z = 2.63$  m, is most strained and limits the fuel cladding operation time at day cycle power maneuvering.

For the WWER-1000 conditions, the rapid creep stage is degenerated when using the Zircaloy-4 cladding corrosion models MATPRO-A and EPRI, at the correcting factor  $COR = -0.431$ . This phenomenon proves that it is possible, for four years at least, to stay at the steady creep stage, where the cladding equivalent creep strain and radial total strain do not exceed 1-2%, on condition that the corrosion rate is sufficiently small.

The WWER-1000 thermal neutron flux axial distribution can be significantly stabilized, at power maneuvering, by means of a proper coolant temperature regime assignment. Assuming the maximum divergence between the instant and equilibrium axial offsets equal to 2%, the regulating unit movement amplitude at constant average coolant temperature is 6%, while the same at constant inlet coolant temperature is 4%. Therefore, when using the method with  $\langle T \rangle = \text{const}$ , a greater regulating unit movement amplitude is needed to guarantee the linear heat rate axial stability, than when using the method with  $T_{in} = \text{const}$ , on the assumption that all other conditions for both the methods are identical.

The WWER-1000 average cladding failure parameter after 500 day cycles, for the most strained sixth axial segment, at power maneuvering according to the method with  $\langle T \rangle = \text{const}$ , is 8.7% greater than the same for the method with  $T_{in} = \text{const}$ , on the assumption that the thermal neutron flux axial distribution stability is identical for both the methods.

The physically based methods of WWER-1000 fuel cladding durability control include: optimal choice of the group of regulating units being used at reactor power maneuvering, balance of stationary and variable loading regimes, choice of fuel element construction and fuel physical properties considering the most strained fuel element axial segment, assignment of the coolant temperature regime and the fuel assembly transposition algorithm.

## 7. References

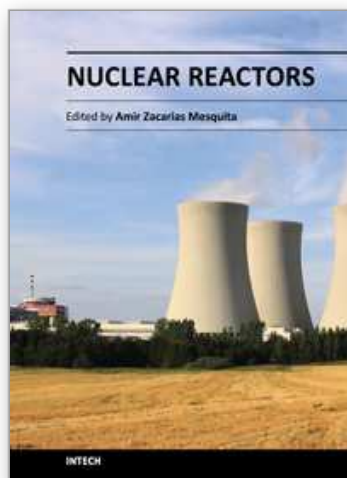
- Bogachev, A.V. et al., 2005. Operating experience of system of the automated control of a residual cyclic resource for RP with VVER-1000. In: Proc. 18-th Int. Conf. on Structural Mechanics in Reactor Technology, Beijing, China.
- Bull, A., 2005. The future of nuclear power, Materials challenges, Birmingham, 21 pp.
- Kesterson, R. L. and Yueh, H. K., 2006. Cladding optimization for enhanced performance margins. In: Proc. Int. Conf. TopFuel, Salamanca.
- Kim, J.H. et al., 2007. Deformation behavior of Zircaloy-4 cladding under cyclic pressurization. Journal of Nuclear Science and Technology 44, 1275–1280.

- Maksimov, M.V. et al., 2009. Model of cladding failure estimation for a cycling nuclear unit. *Nuclear Engineering and Design* 239, 3021–3026.
- Maksimov, M.V. and Pelykh, S.N., 2009. Comparison of fuel-element cladding durability for a WWER-1000 reactor operating in the mode of variable loadings. *Odes'kyi Natsional'nyi Politechnichniy Universytet. Pratsi* 1, 49–53 (in Russian).
- Maksimov, M.V. and Pelykh, S.N., 2010. Method for evaluating the service life of VVER-1000 fuel-element cladding in different loading regimes. *Atomic Energy*. 5, 357–363.
- MATPRO-09, 1976. A Handbook of Materials Properties for Use in the Analysis of Light Water Reactor Fuel Rod Behavior, USNRC TREE NUREG-1005.
- Nemirovskiy, Y., 2001. About an estimation of construction safe operation time, *Proc. Int. Conf. RDAMM-2001*, Novosibirsk, 328 - 333 (in Russian).
- Novikov, V. V. et al., 2005. Nuclear fuel operability assurance in maneuver regimes. In: *Proc. Ukrainian-Russian Conf. on Experience of the new WWER fuel exploitation*, Khmel'nitskiy, p. 22 (in Russian).
- Pelykh, S.N. et al., 2008. Model of cladding failure estimation under multiple cyclic reactor power changes. In: *Proc. of the 2-nd Int. Conf. on Current Problems of Nuclear Physics and Atomic Energy*, Kiev, Ukraine.
- Pelykh, S.N. et al., 2009. A complex power maneuvering algorithm efficiency criterion for a WWER-1000 reactor working in the mode of variable loadings. *Odes'kyi Natsional'nyi Politechnichniy Universytet. Pratsi* 2, 53–58 (in Russian).
- Pelykh, S.N. et al., 2010. Estimation of local linear heat rate jump values in the variable loading mode. In: *Proc. of the 3-rd Int. Conf. on Current Problems of Nuclear Physics and Atomic Energy*, Kiev, Ukraine.
- Pelykh, S.N. and Maksimov, M.V., 2011. Cladding rupture life control methods for a power-cycling WWER-1000 nuclear unit. *Nuclear Engineering and Design* 241, 2956–2963.
- Philimonov, P.E. and Mamichev, V.V., 1998. The "reactor simulator" code for modelling of maneuvering WWER-1000 regimes. *Atomnaya Energiya* 6, 560–563 (in Russian).
- Philipchuk, E. V. et al., 1981. Control of the nuclear reactor neutron field, *Energoatomizdat*, Moscow, 280 pp. (in Russian).
- SCDAP/RELAP5/MOD2, 1990. Code manual, Vol. 4. MATPRO-A: A Library of Materials Properties for Light Water Reactors Accident Analysis, NUREG/CR-5273.
- Semishkin, V.P., 2007. Calculation-experimental methods to ground the WWER fuel element and fuel assembly behaviour under the LOCA emergency conditions. Author's abstract of dissertation for a degree of Doctor of Technical Science, Moscow, 48 p (in Russian).
- Semishkin, V.P. et al., 2009. Standard durability and reliability requirements for WWER reactor unit elements, and safety problems. In: *Abs. of the 6-th Int. Conf. on Safety Assurance of NPP with WWER*, Podolsk, Russia, p. 119 (in Russian).
- Shmelev, V.D. et al., 2004. The WWER active cores for nuclear stations, *Akademkniga*, Moscow, 220 pp. (in Russian).
- Sosnin, O., Gorev, B.V., 1986. Energy Variant of the Theory of Creep, The Siberian Branch of the Russian Academy of Sciences, Novosibirsk, 95 pp. (in Russian).

- Suzuki, M., 2000. Light Water Reactor Fuel Analysis Code FEMAXI-V (Ver.1). JAEA Report, Japan Atomic Energy Research Institute, 285 pp.
- Suzuki, M., 2010. Modelling of light-water reactor fuel element behaviour in different loading regimes, Astroprint, Odessa, 248 pp. (in Russian).

IntechOpen

IntechOpen



## **Nuclear Reactors**

Edited by Prof. Amir Mesquita

ISBN 978-953-51-0018-8

Hard cover, 338 pages

**Publisher** InTech

**Published online** 10, February, 2012

**Published in print edition** February, 2012

This book presents a comprehensive review of studies in nuclear reactors technology from authors across the globe. Topics discussed in this compilation include: thermal hydraulic investigation of TRIGA type research reactor, materials testing reactor and high temperature gas-cooled reactor; the use of radiogenic lead recovered from ores as a coolant for fast reactors; decay heat in reactors and spent-fuel pools; present status of two-phase flow studies in reactor components; thermal aspects of conventional and alternative fuels in supercritical water-cooled reactor; two-phase flow coolant behavior in boiling water reactors under earthquake condition; simulation of nuclear reactors core; fuel life control in light-water reactors; methods for monitoring and controlling power in nuclear reactors; structural materials modeling for the next generation of nuclear reactors; application of the results of finite group theory in reactor physics; and the usability of vermiculite as a shield for nuclear reactor.

### **How to reference**

In order to correctly reference this scholarly work, feel free to copy and paste the following:

Sergey Pelykh and Maksim Maksimov (2012). Theory of Fuel Life Control Methods at Nuclear Power Plants (NPP) with Water-Water Energetic Reactor (WWER), Nuclear Reactors, Prof. Amir Mesquita (Ed.), ISBN: 978-953-51-0018-8, InTech, Available from: <http://www.intechopen.com/books/nuclear-reactors/theory-of-fuel-life-control-methods-at-nuclear-power-plants-npp-with-water-water-energetic-reactor-w>

**INTECH**  
open science | open minds

### **InTech Europe**

University Campus STeP Ri  
Slavka Krautzeka 83/A  
51000 Rijeka, Croatia  
Phone: +385 (51) 770 447  
Fax: +385 (51) 686 166  
[www.intechopen.com](http://www.intechopen.com)

### **InTech China**

Unit 405, Office Block, Hotel Equatorial Shanghai  
No.65, Yan An Road (West), Shanghai, 200040, China  
中国上海市延安西路65号上海国际贵都大饭店办公楼405单元  
Phone: +86-21-62489820  
Fax: +86-21-62489821

© 2012 The Author(s). Licensee IntechOpen. This is an open access article distributed under the terms of the [Creative Commons Attribution 3.0 License](https://creativecommons.org/licenses/by/3.0/), which permits unrestricted use, distribution, and reproduction in any medium, provided the original work is properly cited.

IntechOpen

IntechOpen